NBSIR 76-836

LOW TEMPERATURE FRACTURE BEHAVIOR OF A Ti-6Al-4V ALLOY AND ITS ELECTRON BEAM WELDS

R.L. Tobler

Cryogenics Division
Institute for Basic Standards
National Bureau of Standards
Boulder, Colorado 80302

April 1976

Prepared for
Kirtland Air Force Base
Albuquerque, New Mexico 87117

NBSIR 76-836

LOW TEMPERATURE FRACTURE BEHAVIOR OF A Ti-6Al-4V ALLOY AND ITS ELECTRON BEAM WELDS

R.L. Tobler

Cryogenics Division
Institute for Basic Standards
National Bureau of Standards
Boulder, Colorado 80302

April 1976

Prepared for
Kirtland Air Force Base
Albuquerque, New Mexico 87117

U.S. DEPARTMENT OF COMMERCE, Elliot L. Richardson, Secretary
James A. Baker, III, Under Secretary
Dr. Betsy Ancker-Johnson, Assistant Secretary for Science and Technology

NATIONAL BUREAU OF STANDARDS, Ernest Ambler, Acting Director

CONTENTS

ABSTRACT

The effects of electron beam (EB) welding on the fracture behavior of a recrystallization annealed, extra-low-interstitial Ti-6Al-4V alloy have been investigated at temperatures in the ambient-to-cryogenic range. Plane strain fracture toughness (K_{Ic}) and subcritical crack growth parameters were measured using compact specimens 10 to 25.4 mm thick. These parameters can be used to predict the safe operating lifetimes of cryogenic pressure vessels and other welded Ti-6Al-4V structures.

Although EB welding transforms the base metal microstructure extensively, its effects on the material's fatigue crack propagation resistance at intermediate stress intensity factors are negligible. The growth rates, da/dN, of fatigue cracks sited in the fusion and heat-affected zones of weldments were temperature insensitive and nearly equivalent to rates for the base metal. However, welding introduces a zone of low fracture toughness at the heat-affected-zone/fusion-zone boundary. The K_{Ic} value for this boundary zone at liquid nitrogen temperature (76 K) was 45 $MN/m^{3/2}$, 16% lower than the base metal. The base metal fracture toughness increases between 4 and 295 K, with an abrupt transition to higher K_{Ic} values occurring at temperatures between 76 and 125 K. Static load cracking, temperature effects, and specimen orientation effects on the fracture behavior of this titanium alloy are central topics of discussion.

Key words: Electron beam welding; fatigue; fracture toughness; low temperature tests; mechanical properties; titanium alloy.

1. INTRODUCTION

As discussed by Johnson [1], Ti-6Al-4V is employed in critical cryogenic applications related to aerospace. Favored for its high strength-to-weight ratio, this alloy has become the principal construction material for the cryogenic pressure vessel components of electrical, propulsion, and reaction control systems. Such pressure vessels are designed using low safety factors ($\sim$ 1.5), and may experience service temperatures as low as 20 K (-423°F); they are usually spherical, and are constructed by welding hemispherical forgings at the equator.

Although welding is essential in fabricating these and other large engineering structures, weld zones represent a potential source of structural weakness. Microcracking or porosity may occur during weld metal solidification, and heat conducted to the base metal may induce microstructural transformations with resultant mechanical property degradation. In the case of Ti-6Al-4V, low ductility and toughness in gas metal-arc or gas tungsten-arc welds can be attributed to oxygen and nitrogen contamination [2]. Thicker sections are necessary to guarantee the structural reliability of a weld if its mechanical properties undermatch those of the base metal.

Disregarding its high cost, electron beam welding offers significant technical advantages compared to arc welding. The kinetic energy of high velocity electrons is converted to intense heat upon collision with the structural component. The highly localized heating produces narrow, moderately tapered, deeply penetrating fusion zones. Consequently, factors such as distortion, residual stress, total heat input, and heat-affected zone sizes are minimized. Also, electron beam welding is performed in vacuum, reducing the possibility of impurity pickup [3].

Tensile and fatigue data for electron beam welds in 25.4 to 50.8 mm thicknesses of Ti-6Al-4V are known from tests at room temperature, but most results describe unflawed specimen behavior [4,5]. Fracture mechanics parameters are needed to predict the low temperature service performance of large structures which cannot be guaranteed to be flaw-free. Such data for an extra-low-interstitial Ti-6Al-4V alloy in the recrystallization annealed condition are presented here. Fracture toughness (K_{Ic}), fatigue crack growth rate (da/dN), and static load cracking parameters are reported for the unwelded and the electron beam welded alloy, at selected temperatures between 295 K (70°F) and 4 K (-453°F).

2. EXPERIMENTAL

2.1 Material

The extra-low-interstitial (ELI) Ti-6Al-4V alloy tested in this study was donated by Beech Aircraft Corporation, Boulder, Colorado. The material was received in the form of a 1 m diameter hemisphere with a 51 mm wall thickness. The hemisphere had been recrystallization annealed at 1200 K (1700°F) for 4h, furnace cooled to 1033 K (1400°F) in 3h, cooled to 756 (900°F) in 3/4 h, and air cooled to room temperature.

A commercial chemical analysis of this alloy is listed in Table 1. Mechanical properties of interest are listed in Table 2. The tensile properties at room and liquid nitrogen temperatures were measured using established techniques [6,7]. The elastic properties, measured by an ultrasonic method [8], were equivalent to the published values for a similar heat.

2.2 Electron Beam Welds

Several pairs of arc-shaped bars were machined from stock and electron beam welded by Chem-Tronics, Inc., Santee, California. Most of these bars were 90 cm in arc length and 3.8 x 5.1 cm in cross-sectional area. Two bars having 18 x 5 cm cross-sectional areas were also welded, but the larger integral heat sink offered by this geometry did not affect the fracture properties.

The double-rabbeted, self-backing, self-aligning, square-groove joint used for these welds is shown in Figure 1a. The workpieces were machined, chemically cleaned, and mounted between aluminum chill plates in a rotary indexing fixture. Circumferential welding was accomplished in vacuum at 4×10^{-2} Pa (3×10^{-4} torr), using tack, penetration, and cosmetic passes. The workpieces were rotated under a vertical electron beam, at a gun-to-work distance of 32.4 cm. Other machine settings, determined from trial runs on scrap pieces, are listed in Table 3. The completed welds were annealed in air at 811 K (1000°F) for 50h, simulating a stress-relief heat treatment that is applied to welded pressure vessels.

A weld cross-section that was etched in an $85H_2O$:10HF:$5HNO_3$ solution is shown in Figure 1b. Large prior beta grains give the 30 mm long, 5 mm wide fusion zone a mottled appearance. The included angle of the fusion zone at central thickness is approximately 5 degrees. Heat-affected zones extend approximately 2 mm above and below the fusion zone.

The fracture specimens were machined such that the flawed seam at the weld root (which is typical for this type of joint preparation) was removed by notching. A compact specimen of the ML orientation (described below) is shown in Figure 1c. Based on commercial ultrasonic inspections and metallographic evidence, these laboratory specimens are representative of production quality electron beam welds.

2.3 Specimens

The compact specimen was chosen because it offered a high K_{Ic} measurement capability for its size [9], and a geometry compatible with that of the welded stock. This standard specimen is described in the ASTM method of test for plane strain fracture toughness of metallic materials, ASTM E-399-74 [10].

Base metal specimens were machined from the unwelded forging; weld specimens, from either of two welded-bar samples. Specimen thickness, B, ranged from 10 to 25.4 mm, and widths, W, ranged from 28 to 50.8 mm, as listed in Table 4. Without exception, the planar specimen dimensions were proportional to W, as described in E-399-74, and knife edges for clip gage retention were machined integral to the notch. The knife edges were usually located at the specimen edge. An exception is the series of base metal specimens referred to in Figure 6 below, where loadline deflection is reported.

2.4 Orientation

Reference axes for specimen orientation are defined in Figure 2. The letter R represents the radial direction of the original forging, while M and L represent circumferential (meridional and latitudinal) directions. Base metal specimens were machined in as many as six orientations, designated RL, LR, RM, MR, LM, or ML. The first letter of each designation identifies the direction normal to the fracture plane; the second letter identifies the direction of crack propagation. Weld specimens were tested only in MR and ML orientations where the cracks propagate radially or equatorially.

2.5 Microstructure

The recrystallization annealed base metal microstructure of primary alpha and intergranular beta (or transformed beta phase) is shown in Figure 3. Although nearly equiaxed, the microstructure viewed along the R axis is distinguishable from those of the M and L axes. The latter microstructures are equivalent, having an average primary alpha grain diameter of approximately 0.013 mm.

A microstructural traverse of the weld is shown in Figure 4. At distances of 4 mm or greater from the fusion zone centerline, the base metal microstructure was unaltered by welding. The outer heat-affected zone (3 to 3.5 mm from the fusion line) etches darkly, while the center of the heat-affected zone shows primary alpha in a highly permutated matrix. Near the heat-affected-zone/fusion-zone boundary, the structure consists of aged acicular alpha. The fusion zone is entirely aged martensitic alpha.

Three critical weld locations were selected for fracture testing: 1) FZ, the fusion zone centerline, 2) HAZ, the center of the heat-affected zone, and 3) HAZB, the macroscopically visible heat-affected-zone/fusion-zone boundary. Notches parallel to the fusion line were sited in the desired zones, after etching each specimen blank. The fatigue cracks subsequently propagated parallel to the notch plane, except in the case of HAZB specimens. The cracks in HAZB specimens propagated along the heat-affected-zone/fusion-zone boundary, even though this was at a 2 to 3 degree angle from the notch plane. In any case, no difficulty was encountered in maintaining the fatigue cracks within their intended zones.

2.6 Procedure

The 100 kN capacity servo-hydraulic testing machine and cryostat that were used to conduct these tests are shown in Figure 5. As previously described [11,12], a vacuum insulated dewar containing a cryogen encapsilates the specimen and clip gage at low temperatures. Test environments included unconditioned laboratory air at 295 K (70°F), ethanol and dry ice at 195 K (-108°F), liquid nitrogen at 76 K (-323°F), and liquid helium at 4 K (-453°F). Temperatures between 195 (-108°F) and 108 K (-200°F) were also obtained, by admitting cold nitrogen vapor to the cryostat. A chromel-constantan thermocouple was attached to the specimen during these tests, and a servo-mechanical temperature controller maintained the specified test temperature to within $\pm$ 3 K. Clip gage sensitivity changed by no more than 1.5% between 295 and 4 K, and the E-399-74 linearity requirements were satisfied.

2.6.1 Fracture

The fracture toughness specimens were precracked at their K_{Ic} test temperatures and fractured at a stress intensity factor increase rate of approximately 1 $MN/m^{3/2}$ per second. The critical stress intensity factors were calculated according to the solution for compact specimens:

$$K_Q = P_Q B^{-1} W^{-1/2} [f(a/W)] \tag{1}$$

where

$$f(a/W) = 29.6\ (a/W)^{1/2} - 185.5\ (a/W)^{3/2} + 655.7\ (a/W)^{5/2} - 1017.0\ (a/W)^{7/2} + 638.9\ (a/W)^{9/2} \tag{2}$$

In these equations, P_Q is the load defined by the secant offset procedure, and a is the average of three crack length measurements at 25, 50, and 75% of specimen thickness (B) [10]. The specimen width, W, is defined in Figure 1c.

A quantitative measure of fracture resistance under linear-elastic conditions, K_{Ic}, is defined operationally by the E-399-74 method. The K_Q measurements constitute K_{Ic} data only if plasticity prior to fracture is negligible, and all other E-399-74 requirements are satisfied. In the tests reported here, the crack front uniformity was satisfactory. However, in tests at room temperature, the specimen sizes failed to satisfy the requirement that:

$$B \geq 2.5\ (K_Q/\sigma_y)^2 \tag{3}$$

where σ_y is the uniaxial yield strength of the material. Nonlinear behavior at room temperature proved unavoidable, because specimens of a thickness meeting Eq. (3) could not be manufactured from the available stock.

Nevertheless, using an elastic-plastic fracture criterion based on the J-integral, meaningful K_{Ic} values were derived for the base metal. For nonlinear-elastic materials, J is the rate of change of potential energy with respect to crack area. The critical value, J_{Ic}, is the value of J required to initiate crack extension. Since the J-integral applies to nonlinear load-deflection behavior, the size criterion of Eq. (3) need not be satisfied for a valid result.

Experimentally, J was evaluated as an energy proportional to the area, A, under the load-loadline deflection curves of 20.3 mm thick compact specimens. The extrapolation procedure outlined by Landes and Begley [13] was used. According to their methods, six nearly identical specimens (a/W = 0.58 $\pm$ 1%) were loaded to cause decreasing amounts of stable crack extension. These six specimens were then unloaded, heat-tinted, and fractured into halves for crack extension measurements. The J values at points of unloading were calculated using the equation [14]:

$$J = \frac{\lambda A}{Bb} \tag{4}$$

where b is the specimen ligament (W-a), and λ is a coefficient greater than 2 and dependent on a/W [14]. The six values of J obtained were plotted versus crack extension and extrapolated to determine J_{Ic}. Finally, K_{Ic} was obtained from the expression:

$$K_{Ic}^2 = \frac{E}{1-\nu^2} \cdot J_{Ic} \tag{5}$$

where E is Young's modulus and ν is Poisson's ratio. Thus, a room temperature K_{Ic} value was estimated, but only for base metal specimens of the LR orientation.

2.6.2 Fatigue

Considerable amounts of fatigue crack growth data were obtained during the precracking of fracture toughness specimens where the maximum fatigue stress intensity factor did not exceed 34 $MN/m^{3/2}$. Additional specimens were tested at 295 and 76 K, solely for fatigue crack growth rates at higher stress intensity factors.

The fatigue tests were conducted under controlled load, using a sinusoidal load cycle at frequencies, F, from 10 to 30 Hz. The ratio, R, of minimum/maximum load was 0.1. A digital indicator was used to continuously monitor the peak loads, which were accurate to $\pm$ 2% of the specified values.

Fatigue crack growth was monitored by elastic compliance or crack opening deflection measurements, an approach based on the fact that deflection per unit load, δ/P, increases with increasing crack length. Correlations between crack length and δ/P were obtained experimentally, using the average crack length measurements of fractured specimens. Changes in clip gage sensitivity and Young's modulus with temperature were accounted for by plotting the base metal data versus EB δ/P, or by shifting the weld specimen room temperature calibration curves [12]. A correlation curve applicable to 20.3 mm thick compact specimens of the base metal (with δ measured at the loadline) is shown in Figure 6.

The crack growth rate measurement procedure involved recording δ-versus-P periodically. Crack lengths, inferred from the empirical correlations, were plotted versus cycles, N. Computer programs were used to fit the a-versus-N curves with a third-order polynomial, to differentiate the curves for da/dN data, and to calculate the corresponding stress intensity factor range, ΔK, from the peak fatigue stress intensity factors:

$$\Delta K = K_{max} - K_{min} \tag{6}$$

2.6.3 Static Load Cracking

A series of specimens were sustained in inert environments at constant load to determine whether time-dependent crack growth culminating in fracture could occur. These base metal (B = 25.4 mm) and weld specimens (B = 10 mm or 17 mm) were precracked as for K_{Ic} testing. Each specimen was loaded within 15 seconds to a specified stress intensity factor. Many

specimens were instrumented with a clip gage so that cracking could be monitored by deflection measurements.

For the base metal specimens, meaningful static load cracking rates were measured by unloading after moderate crack extensions of no more than 2 mm. The test procedure involved: 1) sustaining the specimens at constant load for hold times, Δt, ranging from 15 to 10^5 seconds, 2) unloading and heat-tinting the specimens to oxidize their crack surfaces, and 3) fracturing the specimens into halves to measure the crack extension. Tinting was accomplished by heating with an acetlyene torch. After specimen fracture, increments of static load crack extension were identifiable as straw-blue oxidized areas located between the fatigue crack and the untinted ligament.

An average crack extension, Δa, was obtained from three measurements with a traveling microscope at 25, 50, and 75% of specimen thickness. The cracking rate, $\Delta a/\Delta t$, for each test was then calculated and plotted versus the nominal value of K at the initial crack length and static load, P_s:

$$K = P_s B^{-1} W^{-1/2} f\left(\frac{a}{W}\right) . \qquad (7)$$

For compact specimens, K increases continuously with crack extension under constant load, and the $\Delta a/\Delta t$-versus-K relationships are only approximate. However, the calculations were performed for Δa values from 1 to 2 mm, and differences between the initial and final K values were not greater than 5%.

3. RESULTS

3.1 Fracture Toughness

Fracture test records for two base metal specimens are shown in Figure 7. These load-deflection curves are typical of weld specimen behavior also. Linearity prior to fast fracture occurred at 76 K, where all K_{Ic} measurements were valid. Nonlinearity and stable crack extension occurred at room temperature, and all tests failed the requirement of Eq. (3). The maximum loads at 295 K exceeded 1.1 P_Q, which also disqualifies the K_Q values as K_{Ic} results. Tables 5-9 list the results at each temperature, along with observations relating to validity requirements. In several cases a/W exceeds 0.55. Although this deviates from the E-399-74 specifications, the K_Q results were not in disagreement with valid K_{Ic} data, as indicated by tests at 76 K. This near equivalence of results is indicated in the tables by the statement $K_Q \overset{\sim}{=} K_{Ic}$.

J-integral data for the base metal at 295 K are shown in Figure 8. Apparently, J varies linearly at crack extensions greater than 0.12 mm. As discussed by Landes and Begley [13], the J_{Ic} measurement point might be selected by several different methods:

1) The curve could be linearly extrapolated to $\Delta a = 0$, identifying J_{Ic} on the ordinate axis as approximately 80 kJ/m^2.

2) A line, $J/2\sigma_y$, may be constructed, its intersection with the J-Δa curve yielding $J_{Ic} \overset{\sim}{=} 88$ kJ/m^2.

3) A 1% crack extension may be defined as critical. In this case, the J-Δa curve indicates that $J_{Ic} \tilde{=} 100$ kJ/m^2.

Summarizing, J_{Ic} for the LR orientation of the base metal at room temperature lies in the range 80 to 100 kJ/m^2 (457 to 571 in-lb./in^2), depending on the method applied to select the measurement point from Figure 8. According to Eq. (5), the corresponding K_{Ic} values for this alloy at room temperature are 99 to 111 MN/m$^{3/2}$.

Fracture toughness results for the base metal are plotted in Figure 9, which includes the room temperature K_{Ic} data derived by J-integral tests. The ML and LR orientations exhibit a similar temperature dependence: between 295 and 125 K, K_{Ic} remains at relatively high shelf levels; but, as the temperature is lowered between 125 and 76 K, a 33 to 45% decrease of K_{Ic} occurs. On further temperature reductions to 4 K, the data for the LR orientation indicate only a slight decline of K_{Ic}. Thus, the recrystallization annealed and furnace cooled Ti-6Al-4V alloy exhibits a fracture toughness transition at low temperatures which resembles the classical fracture transitions of other metals and alloys having body-centered cubic or hexagonal crystal structures. The abrupt decrease of K_{Ic} in the interval 76 K < T < 125 K suggests that a change in the micromode of fracture occurs, but there was no attempt to verify this fractographically.

Some anisotropy in the fracture toughness data is evident at temperatures above the transition region. The shelf K_{Ic} values for the LR orientation range from 100 to 110 MN/m$^{3/2}$, while shelf values for the ML orientation average approximately 15% lower. These orientation effects become immeasurable at temperatures within the transition range or below. The data for six orientations at 76 K are listed in Table 7 and bracketed in Figure 9. At this temperature any effects due to orientation are indistinguishable from the scatter of replicate tests, although it may be significant to note that the RL orientation yielded two of the lowest K_{Ic} values. Neglecting any minor effects, the nineteen results at 76 K can be statistically described: the mean value of K_{Ic} at this temperature is 60.8 MN/m$^{3/2}$, the K_{Ic} values range between 54.6 and 65.9 MN/m$^{3/2}$, and the standard deviation is 3.0.

Other results in Table 8 indicate that stress-relief heat treatments such as applied to welded structures (533 or 811 K, 50h, air cool) do not lower the base metal fracture toughness. However, prestraining at room temperature can reduce the toughness of Ti-6Al-4V by as much as 50%, while virtually eliminating the temperature dependence of K_{Ic} over the ambient-to-cryogenic range. This point is emphasized in Figure 10 and clarified in discussion.

Electron beam welding also lowers the fracture toughness of this Ti-6Al-4V alloy. The weld data are listed in Table 9, and the average K_Q and K_{Ic} values at 295 and 76 K are compared in Figure 11. The fusion and heat-affected zones at 76 K are nearly equivalent, with K_{Ic} averaging 4 to 6% lower than the 60.8 MN/m$^{3/2}$ value for the base metal. However, a zone of minimum toughness is located at the heat-affected-zone/fusion-zone boundary; there, K_{Ic} for three specimens at 76 K ranged from 47.5 to 53.1 MN/m$^{3/2}$, averaging 16% lower than the base metal.

3.2 Fatigue Crack Growth Rates

Fatigue crack growth rates for the base metal at 295, 195, 76 and 4 K are shown in Figures 12 and 13. These data were obtained from specimens of the LR and ML orientations, as noted. Additional data for RL, LM, MR and RM orientations were obtained at 76 K during precracking of the K_{Ic} test specimens of Table 8. These additional data, obtained at ΔK values between 22 and 32 $MN/m^{3/2}$, fall within the scatterbands of Figures 12 and 13. A comparison of all results shows no measurable specimen orientation or temperature effects over the range of ΔK investigated.

Fatigue crack growth in electron beam welds was investigated at two temperatures. As indicated in Figures 14 and 15, cracks were propagated in the fusion, heat-affected, and boundary zones at 295 and 76 K. Again, it appears that any temperature effects are insignificant compared to the scatter observed in replicate tests.

The scatterbands of Figures 12-15 are superimposed for comparison in Figure 16. The unshaded band represents the base metal results of Figures 12 and 13 combined. The bands for weld data are nearly equivalent in width, and nearly coincide with the base metal band. Thus, despite the microstructural transformations that are introduced, electron beam welding has little effect on the fatigue crack propagation resistance of this alloy. The fatigue crack growth rates of Ti-6Al-4V are virtually structure insensitive for the ΔK ranges investigated.

The linear trend of data on logarithmic coordinates is in accord with the equation proposed by Paris and Erdogan [15], namely:

$$\frac{da}{dN} = C(\Delta K)^n \quad . \tag{8}$$

Here C and n are empirical constants which can be determined graphically. A line approximation conforming to this equation and favoring the upper bound of crack growth rates is shown in Figure 16. The value of C, the intercept on the ordinate axis at $\Delta K = 1$, is 2.7×10^{-9} mm/cycle; the slope, n, is 3.7. Of course, other linear approximations could be chosen for specific applications of these data.

3.3 Static Load Cracking (SLC)

Several aspects of static load cracking in the base metal are illustrated by the test record and fracture surface of Figure 17. The deflection at constant load reflects time-dependent crack extension which is most pronounced at the center of the specimen thickness (plane strain conditions). Crack extension at the specimen edges (plane stress conditions) is retarded. Judging from the regular increase of deflection, cracking in the base metal began without delay; i.e., no incubation periods were observed in tests at 295, 195, or 130 K. In two tests at 295 K, cracking led to complete fracture when the initial load was maintained indefinitely. The phenomenon occurs at stress intensity factors well below the "critical" levels associated with P_Q or the maximum loads of E-399-74 fracture test records.

The base metal cracking rates are highly sensitive to the applied stress intensity factor. The rates can be described as power law functions of K, having the form:

$$\frac{\Delta a}{\Delta t} = B(K)^m \tag{9}$$

Here, B and m, empirical constants that depend on temperature, were graphically determined from Figure 18, using SI units. At room temperature,

$$\frac{\Delta a}{\Delta t} = 1.9 \times 10^{-56} (K)^{27} \tag{10}$$

and, at 195 K,

$$\frac{\Delta a}{\Delta t} = 4.3 \times 10^{-72} (K)^{36} \tag{11}$$

As indicated in Figure 18, the rates at 195 K exhibit less scatter and are faster than those at room temperature. To demonstrate that these effects are not due to stress corrosion, the chemistry of the environment was alternated. The cracking rates for two specimens submerged in ethanol at 295 K were not higher than those in room air. Similarly, the data at 195 K are in excellent agreement, regardless of whether the environment was nitrogen vapor or a mixture of alcohol and dry ice. Therefore, the environments used here are believed to be chemically inert.

Although the data at 130 K are few, they clearly indicate a decrease in static load cracking rates between 195 K and 130 K. Thus, the rates do not vary monotonically with temperature, but peak at some temperature between 295 K and 130 K. One possible explanation for this trend is a change in the micromode of cracking, as suggested in the discussion.

Three room temperature specimens tested at constant stress intensity factors ranging from 52 to 60 $MN/m^{3/2}$ showed no evidence of cracking after hold times of 116h. Accordingly, 60 $MN/m^{3/2}$ can be taken as the apparent room temperature value of K_{Th}, the threshold stress intensity factor below which static load cracking was not observed in 116h tests. Since all of the base metal SLC specimens were of the ML orientation, the ratio of K_{Th}/K_{Ic} at room temperature is estimated to be 0.7.

Note that the static load cracking rates are less sensitive to temperature variations at lower K. If the linear trends of Figure 18 are extrapolated, they appear to converge at $K \tilde{=} 63$ $MN/m^{3/2}$. This prompts a speculation that K_{Th} may not vary greatly with temperature, but additional experiments would be necessary to establish K_{Th} values with confidence.

Static load tests were also performed on specimens submerged in liquid nitrogen at 76 K. Three base metal specimens were loaded for 10 to 16h at K/K_{Ic} ratios from 90 to 96%. As verified by heat-tinting, crack growth did not occur under these conditions. The absence of cracking at 76 K may be viewed as a continuation of the declining trend observed below 195 K. Such results are consistent with the hypothesis that static load cracking is a thermally activated process which can be suppressed at sufficiently low temperatures.

Fusion zone and heat-affected-zone boundary specimens from electron beam welds were subjected to static load tests at 76 K and 295 K. As noted earlier, the stock dimensions dictated the use of specimens smaller than the 25.4 mm thickness favored for the base metal, and a 10 mm weld specimen thickness was selected.

At 76 K, duplicate specimens from the weld zones were sustained for up to 16h at K/K_{Ic} ratios between 90 and 98%. The results showed no evidence of static load cracking at this temperature.

The weld specimens did exhibit cracking at room temperature, but the behavior differed from that of the base metal. Table 10 summarizes the results. For example, an unknown amount of stable crack extension occurred during loading to the initial K value. A crack extension of 0.07 mm was measured after heat-tinting one fusion zone specimen which had been subjected to a K value of 64 $MN/m^{3/2}$ and promptly unloaded. Thus, not all of the crack extension in static tests could be attributed to static load cracking. Also, crack arrest occurred in tests of the fusion zone, while fast fracture occurred at the HAZ/FZ boundary. For these reasons, meaningful crack growth rates could not be calculated for weld specimens.

The heat-affected zone boundary seems critical with respect to static load cracking resistance. One room temperature HAZB specimen fractured at an initial stress intensity factor of 60.4 $MN/m^{3/2}$, a level which had proved innocuous to base metal and fusion zone specimens. Presumably, the greater susceptibility to static load cracking at the heat-affected zone boundary relates to the fact that the K_Q and K_{Ic} values are lowest there as well. Unfortunately, the scatter in results for HAZB specimens at room temperature is considerable. Good estimates of K_{Th} require hold times greater than 100h.

Finally, there is evidence that an incubation period precedes cracking in the HAZ/FZ boundary specimens. A delay of 10^3 s was noted in one test during which there was no sign of any crack growth; subsequently, an increase of clip gage deflection signaled the onset of cracking and fracture followed within an additional 20 s. Another specimen showed no time-dependent crack extension at all, but fractured spontaneously after 20 s at a stress intensity factor of 69.9 $MN/m^{3/2}$. These observations suggest that different mechanisms may govern static load cracking in base and weld metal specimens.

4. SUMMARY

The fracture behavior of a recrystallization annealed and furnace cooled extra-low-interstitial Ti-6Al-4V alloy and its electron beam welds is summarized as follows:

1) Fracture toughness: At temperatures between 4 and 295 K, K_{Ic} for this alloy ranges from 54 to 105 $MN/m^{3/2}$. An abrupt transition in K_{Ic} values occurs between 76 to 125 K. There is a slight degree of fracture anisotropy, but only at temperatures above the transition region. Electron beam welding leads to a 16% decrease in K_{Ic} at 76 K, the heat-affected-zone/fusion-zone boundary being the region of minimum fracture toughness in an electron beam weld.

2) Fatigue crack growth rates: Within the scatter of replicate tests, and over the ΔK ranges investigated, the fatigue crack propagation resistance of this alloy is insensitive to specimen orientation, temperature, and microstructural transformations due to welding. A single equation favoring the upper bound of the fatigue crack growth rates (mm/cycle) as a function of ΔK ($MN/m^{3/2}$) is:

$$\frac{da}{dN} = 2.7 \times 10^{-9} (\Delta K)^{3.7} \qquad (12)$$

3) Static load cracking: Precracked base and weld metal specimens sustained at stress intensity factors approaching K_{Ic} did not exhibit static load cracking in liquid nitrogen environments at 76 K. However, static load cracking did occur in inert environments at temperatures between 130 and 295 K. Cracking in the base metal begins without delay at K values greater than 60 $MN/m^{3/2}$. The HAZ/FZ specimens exhibit an incubation period prior to cracking, suggesting that a different mechanism is operative. The degradation in fracture resistance due to the possibility of fracture under static loading can amount to 30%.

5. DISCUSSION

Campbell's review [16] of low temperature fracture behavior reveals few valid data for titanium alloys. The existing literature does not associate transitional fracture behavior with Ti-6Al-4V alloys, but asserts that K_{Ic} decreases uniformly at low temperatures. Certainly, the normal grades having relatively high carbon, oxygen, nitrogen, and hydrogen contents exhibit low K_{Ic} values (35 to 43 $MN/m^{3/2}$) and mild temperature dependences [12,17]. But why were transitions for extra-low-interstitial Ti-6Al-4V alloys not previously reported? Among other factors, the interval 76 K < T < 125, was never previously investigated, and invalid results predating current testing standards sometimes obscured the true trend of K_{Ic} [18-20].

Invalid fracture data must be cautiously interpreted, for it has been demonstrated that K_Q results are specimen size dependent, and of limited use for comparative or design purposes. Some evidence for titanium alloys, including Ti-6Al-4V, indicates that K_Q increases with specimen dimensions [21-23]. The present results for the base metal at room temperature, when compared directly with Annis' data [24], show that K_Q increases from 67 to 83 to 93 $MN/m^{3/2}$ as compact specimen thickness (W/B = 2) increases from 12.5 to 20.3 to 25.4 mm. In view of this size dependence, the finding that room temperature K_Q values realistically rank the fracture toughness of welds, as shown in Figure 11, may be fortuitous. Only K_{Ic} data legitimately establish a ranking.

Although specimen orientation effects were noted in the K_{Ic} data at temperatures above the transition region, this alloy is nearly isotropic compared to most rolled or forged alloys. Considering the equiaxed nature of the recrystallized base metal microstructure as revealed in Figure 3, one appreciates that several orientations tested here were virtually equivalent.

Nevertheless, we can only assume that slight microstructural dissimilarities account for the anisotropy noted in Figure 9. It is not inconsistent to report no measurable orientation effects at low temperatures, in view of the implied change in fracture mode. Analogously, fracture anisotropy in steels is most pronounced at temperatures above the transition region [25].

The virtual independence of fatigue crack growth rates with respect to temperature is supported by other work on Ti-6Al-4V alloys. The mill-annealed normal grades tested by Fowlkes and Tobler [12] and Wei and Ritter [26] show no measurable differences in rates at temperatures ranging from 4 to 563 K. Pittinato's data [27] for an ELI grade tested in gaseous helium also show little effect of temperature in the range 145 to 295 K. Evidently, there is no correlation between K_{Ic} and da/dN; the former property varies sensitively with temperature, while the latter does not.

Microstructural effects on fatigue crack growth in titanium alloys are poorly understood. Yoder, Cooley, and Crooker [28] reported that a beta-annealed commercial purity Ti-6Al-4V base metal microstructure offers superior resistance, with rates that are up to 10 times slower than the same material in the mill-annealed condition. Figure 16 demonstrates that the EB weld fusion zone and base metal fatigue crack growth rates are virtually identical, despite the fact that these two zones contain aged martensitic alpha and equiaxed alpha microstructures, respectively. Similarly, Irving and Beevers [28] tested five microstructures of a Ti-6Al-4V alloy and concluded that the fatigue crack growth rates were structure-insensitive at ΔK values greater than 12 $MN/m^{3/2}$. The present results are in harmony with Johnson and Paris' statement [30] that structure exerts only a secondary influence on da/dN. In any event, microstructure and temperature effects may become quite significant at ΔK values below 12 $MN/m^{3/2}$, or at relatively high ΔK values approaching K_{Ic} [29,31]. Therefore, the statements in this report regarding fatigue crack growth behavior apply strictly to the intermediate range of ΔK investigated.

Static load cracking in titanium alloys at temperatures below the secondary creep regime (i.e., at test temperature/melting-point ratios, T/T_m, of less than 0.4) is not completely understood [32-35]. A successful theory must rationalize several observations: that the resistance to fracture under static loading is reduced by electron beam welding, that different mechanisms are involved in base and weld metal specimens, and that cracking rates at low temperatures (195 K) may be more severe than at room temperature.

At the 50 ppm level of the present alloy, interstitial hydrogen may facilitate cracking by diffusing to and concentrating at regions of high stress [35-38]. Local fracturing is assisted by reductions of fracture surface energy and cohesive strength. It is also known that primary creep occurs in Ti-6Al-4V alloys, at stress levels as low as 70% of the conventional yield strength [39]. Thus, primary creep in the crack-tip plastic zone of a compact specimen at room temperature is expected. If we accept the theories that interstitial hydrogen and creep effects are responsible for static load cracking in Ti-6Al-4V, it follows from the present results at 130 K that these processes must be operative at T/T_m ratios as low as 0.07.

If static load cracking is governed by thermally activated processes involving diffusion or creep, one might expect crack growth rates to decrease with decreasing temperature. Clearly, the base metal data at temperatures between 295 K and 195 K (Figure 18) do not follow the expected trend.

Rationalizations for the increase in static crack growth rates between 295 and 195 K postulate a change in the micromode of fracture. Static load cracking in Ti-6Al-4V at room temperature involves mixed modes of dimpled rupture and cleavage [35]. Possibly, an increased constraint to plasticity at 195 K favors cleavage and higher cracking rates. Varying tendencies to crack branching may also play a role. Such effects, superimposed on those of a thermally activated process, would explain an otherwise unpredicted temperature dependence.

6. RECOMMENDATIONS

Gowan and Stein described the fracture of a Ti-6Al-4V pressure vessel which was destructively tested at room temperature [40]. There was a sizeable volumetric expansion prior to fracture, and postmortem tests confirmed that the burst-tank material had been strain-hardened [41]. Fracture tests of material taken from the deformed and fractured tank were shown in Table 6 and Figure 9. Clearly, the burst-tank material properties are not representative of the Ti-6Al-4V alloy in its annealed condition, and the data for prestrained material are useless in fracture mechanics evaluations of existing structures.

Electron beam welding reduces the K_{Ic} and K_{Th} values of the material in a region near the macroscopically visible HAZ/FZ boundary. The minimum cycle-life of a welded structure of constant geometry and thickness would be calculated by assuming that a flaw exists at this boundary zone. However, if thick weld lands are employed to reduce the stresses in welds, the base metal properties may be critical. Thus, structural failures may not necessarily initiate in the welds [40].

At temperatures of 76 K or lower, K_{Ic} is a conservative design criterion, since static load cracking is improbable. At room temperature, neither K_{Ic} nor K_Q are conservative design criteria since static load crack growth in flawed structures occurs at lower stress intensity factors. To account for this possibility, fracture mechanics evaluations at room temperature should employ K_{Th}, rather than K_{Ic}, as the critical stress intensity never to be exceeded in structures during service.

The reliability of a K_{Th} measurement increases at very long hold times [34]. In the absence of rigorously determined K_{Th} values for the base metal, eqs. (10) and (11) can be used to make conservative predictions of static load cracking resistance. Assuming these equations hold at lower K values, the time required to produce measurable crack growth at a given temperature and stress intensity factor level can be calculated. For $K < 55\ MN/m^{3/2}$, the time required for significant crack growth should exceed the service lifetimes of most Ti-6Al-4V structures.

Since the attempt to develop static load crack growth rate expressions for weld specimens failed, an alternative test procedure aimed at direct determination of K_{Th} is recommended. The procedure described by Novak and Rolfe [42], whereby numerous specimens are bolt-loaded for long periods, could be adopted for this purpose. Testing should concentrate on the heat-affected zone boundary region where K_{Th} values are evidently lowest.

The possibility of optimizing the fracture resistance of this alloy should also be considered. It proved feasible to enhance the utility of steels by shifting or eliminating their transition temperatures by grain size, heat treatment, or compositional modifications. Similar effects for Ti-6Al-4V might be investigated with the intention of obtaining higher K_{Ic} values at temperatures below 125 K, while improving the resistance to static load cracking at higher temperatures. Data for related titanium alloys suggest that an increased cooling rate from the annealing temperature may influence these properties substantially [43,44].

7. ACKNOWLEDGMENTS

This final report describes work sponsored by Kirtland Air Force Base, under Kirtland Order AFWL 75-177. The assistance of H. Vail (Chem-Tronics, Inc.) in providing the electron beam welds and related technical information is gratefully acknowledged. The assistance of E. Ballinger and S. Naranjo in fracture testing and data reduction is also deeply appreciated.

8. REFERENCES

1. R. E. Johnson, Titanium alloy pressure vessels in the manned space program, in The Science, Technology, and Application of Titanium, p. 1175, R. I. Jaffee and N. E. Promisel, Eds. (Pergamon, London, 1969).

2. S. S. White and R. Bakish, Electron beam welding, Chapter 9 in Introduction to Electron Beam Technology, R. Bakish, Ed. (Wiley, New York, 1962).

3. M. G. Bennett, High voltage electron beam welding of titanium alloys in partial vacuum, in The Science, Technology and Application of Titanium, p. 1023, R. I. Jaffee and N. E. Promisel, Eds. (Pergamon, London, 1969).

4. C. A. Stubbington and J. T. Ballett, Weld optimization and fatigue tests on low voltage electron beam welded 2 in (51 mm) thick Ti-6Al-4V alloy, in Titanium Science and Technology, p. 601, R. I. Jaffee and H. M. Hurte, Eds. (Plenum, New York, 1975).

5. M. T. Groves and J. M. Gerken, Evaluation of electron beam welds in thick materials, in Electron and Ion Beam Science and Technology, p. 477, R. Bakish, Ed. (Wiley, New York, 1966).

6. Tension testing of metallic materials, E8-72, Annual Book of ASTM Standards, Part 31 (Amer. Soc. Test. Mater., Philadelphia, 1973).

7. R. P. Reed, A cryostat for tensile tests in the temperature range 300 to 4 K, in Adv. in Cryog. Engrg. 7, p. 448, K. D. Timmerhaus, Ed. (Plenum, New York, 1962).

8. E. R. Naimon, W. F. Weston, and H. M. Ledbetter, Elastic properties of two titanium alloys at low temperatures, Cryogenics 14, 245-249 (1974).

9. J. E. Srawley and W. F. Brown, Jr., Plane strain crack toughness testing of high strength metallic materials, ASTM STP 410 (Amer. Soc. Test. Mater., Philadelphia, 1969).

10. Standard method of test for plane strain fracture toughness of metallic materials, E-399-74, Annual Book of ASTM Standards, Part 10 (Amer. Soc. Test. Mater., Philadelphia, 1974).

11. R. L. Tobler, Fatigue crack growth and J-integral fracture parameters for Ti-6Al-4V at ambient and cryogenic temperatures, presented at the Ninth National Symposium on Fracture Mechanics, University of Pittsburgh (August, 1975).

12. C. W. Fowlkes and R. L. Tobler, Fracture testing and results for a Ti-6Al-4V alloy at liquid helium temperatures, Eng. Fract. Mech., submitted for publication.

13. J. D. Landes and J. A. Begley, Test results from J-integral studies: an attempt to establish a J_{Ic} test procedure, in Fracture Analysis, ASTM STP 560, p. 170 (Amer. Soc. Test. Mater., Philadelphia, 1974).

14. J. G. Merkle and H. T. Corten, A J-integral analysis of the compact specimen, considering axial force as well as bending, J. Pressure Vessel Tech., Trans. ASME, No. 6, 1-7 (1974).

15. P. C. Paris and F. Erdogan, A critical analysis of crack propagation laws, J. Basic Eng., Trans. ASME, Series D, 85, 528-534 (1963).

16. J. E. Campbell, Fracture toughness of high strength alloys at low temperature-a review, in Fatigue and Fracture Toughness-Cryogenic Behavior, ASTM STP 556, p. 3 (Amer. Soc. Test. Mater., Philadelphia, 1974).

17. C. Vishnevsky and E. A. Steigerwald, Fracture toughness of some cryogenic materials at room and subzero temperatures, in Fracture Toughness Testing at Cryogenic Temperatures, ASTM STP 496, p. 3 (Amer. Soc. Test. Mater., Philadelphia, 1970).

18. W. E. Witzell, Fracture data for materials at cryogenic temperatures, Tech. Rept. AFML-TR-67-257, General Dynamics-Convair, AD 825264 (1967).

19. C. F. Tiffany and P. M. Lorenz, An investigation of low cycle fatigue failure using applied fracture mechanics, Tech. Doc. Rept. ML-TDR-64-53, Boeing (1964).

20. L. R. Hall, Plane-strain cyclic flaw growth in 2014-T62 aluminum and 6Al-4V (ELI) titanium, N69-20265, NASA-CR-62396, Boeing (1968).

21. M. J. May, British experience with plane strain fracture toughness testing, in Review of Developments in Plane Strain Fracture Toughness Testing, ASTM STP 463, p. 41 (Amer. Soc. Test. Mater., Philadelphia, 1970).

22. D. Munz, K. H. Galda, and F. Link, Effect of specimen size on fracture toughness of a titanium alloy, in Mechanics of Crack Growth, ASTM STP 590 (Amer. Soc. Test. Mater., Philadelphia, 1976).

23. H. I. McHenry and R. E. Key, Brazed titanium fail-safe structures, Welding Journal 53, 432-439S (1974).

24. C. G. Annis, Fracture toughness evaluation of Ti-6Al-4V taken from the ALL cryogenic storage assembly forging, memorandum to D. R. Cornnell, Pratt and Whitney Aircraft, Florida Research and Development Center (June, 1975).

25. J. F. Knott, Fundamentals of Fracture Mechanics (Butterworth, London, 1973).

26. R. P. Wei and D. L. Ritter, The influence of temperature of fatigue-crack growth in a mill annealed Ti-6Al-4V alloy, J. Mater. 7, 240-250 (1972).

27. G. F. Pittinato, Hydrogen-enhanced fatigue crack growth in Ti-6Al-4V weldments, Met. Trans. 3, 235-243 (1972).

28. G. R. Yoder, L. A. Cooley, and T. W. Crooker, Metallurgical optimization of a commercial purity Ti-6Al-4V alloy, Rept. NRL Prog., 16-19 (1975).

29. P. E. Irving and C. J. Beevers, Microstructural influences on fatigue crack growth in Ti-6Al-4V, Mater. Sci. Eng. 14, 229-238 (1974).

30. H. H. Johnson and P. C. Paris, Subcritical flaw growth, Eng. Fract. Mech. 1, 3-45 (1968).

31. T. W. Crooker, The role of fracture toughness in low-cycle fatigue crack propagation for high-strength alloys, Eng. Fract. Mech. 5, 35-43 (1973).

32. G. R. Yoder, C. A. Griffis, and T. W. Crooker, The cracking of Ti-6Al-4V alloys under sustained load in ambient air, J. Eng. Mater. Tech., Trans. ASME, Series H, 96, 268-274 (1974).

33. D. N. Williams, Effect of specimen thickness on subcritical crack growth under sustained load, Mater. Sci. Eng. 18, 149-155 (1975).

34. D. N. Williams, Subcritical crack growth under sustained load, Met. Trans. 5, 2351-2358 (1974).

35. D. A. Meyn, Effect of hydrogen on fracture and inert-environment sustained load cracking resistance of α-β titanium alloys, Met. Trans. 5, 2405-2414 (1974).

36. A. R. Troiano, The role of hydrogen and other interstitials in the mechanical behavior of metals, Trans. ASM 52, 54-80 (1960).

37. W. W. Gerberich and Y. T. Chen, Hydrogen controlled cracking--an approach to threshold stress intensity, Met. Trans. 6A, 271-278 (1975).

38. H. W. Liu, Stress-corrosion cracking and the interaction between crack-tip stress field and solute atoms, J. Basic Eng., Trans. ASME, Series D, 92, 633-638 (1970).

39. B. C. Odegard and A. W. Thompson, Low temperature creep of Ti-6Al-4V, Met. Trans. 5, 1207-1213 (1974).

40. J. G. Gowan and C. Stein, Metallographic analysis of fracture surfaces of the 20.7 Cu. Ft. pressure vessel for the ALL cryogenic storage assembly, presented at the Titanium Materials Properties Seminar, Kirtland AFB, Albuquerque, New Mexico (February, 1975).

41. P. J. Bania, Ti-6Al-4V pressure vessel toughness evaluation, presented at the Titanium Materials Properties Seminar, Kirtland AFB, Albuquerque, New Mexico (February, 1975).

42. S. R. Novak and S. T. Rolfe, Modified WOL specimen for K_{ISCC} environmental testing, J. Mater. JMLSA 4, 701-728 (1969).

43. R. H. Van Stone, J. R. Low, Jr., and J. L. Shannon, Jr., The effect of microstructure on the fracture toughness of titanium alloys, NASA Tech. Rept. No. 2-Ti, Department of Metallurgy and Materials Science, Carnegie-Mellon University, Pittsburgh, PA, and National Aeronautics and Space Administration, Lewis Research Center, Cleveland, OH (December, 1974).

44. R. E. Lewis, J. G. Bjeletich, T. M. Morton, and F. A. Crossley, Effect of cooling rate on fracture behavior of mill-annealed Ti-6Al-4V, presented at the Ninth National Symposium on Fracture Mechanics, University of Pittsburgh (August, 1975).

Table 1. Mill analysis (wt %) of extra-low-interstitial, recrystallization annealed Ti-6Al-4V.

Ti	Al	V	Fe	O	C	N	H
Balance	5.91	3.94	0.103	0.110	0.018	0.014	52 ppm

Table 2. Mechanical properties.

Temperature K (°F)	0.2% Yield Strength MN/m^2	(ksi)	Ultimate Strength MN/m^2	(ksi)	Elongation (%)	Red. Area (%)	Young's Modulus GN/m^2 (10^6 psi)	Poisson's Ratio [15]
295 (70)	830	(120.5)	890	(129.1)	14	41.2	1.11 (16.1)	0.323
76 (-323)	1363	(197.7)	1429	(207.3)	9.6	16.4	1.21 (17.5)	0.310

Table 3. Electron beam welding variables.

Operation	Accelerating Voltage (kv)	Beam Current (mA)	Focus	Travel Speed mm/s (in/s)
Tack pass	115	15	Sharp	4.8 (0.189)
Penetration pass[a]	150	45	Sharp	4.8 (0.189)
Cosmetic pass[a]	120	25	Sharp, + 100	3.5 (0.138)

[a] Using two complete revolutions (720°) of the workpiece.

Table 4. Test program and compact specimen descriptions.

Crack Location		Test Type[a]			Specimen Thickness, B		Specimen Width, W		Width-to-Thickness Ratio
		K_{Ic}	$\frac{da}{dN}$	SLC	mm	(inch)	mm	(inch)	
Base Metal	1	X	X	X	25.4	(1.0)	50.8	(2.0)	2
	2	X	X	-	20.3	(0.8)	40.6	(1.6)	2
Electron Beam Weld									
Fusion zone	1	X	X	X	14	(0.55)	28	(1.10)	2
	2	X	-	-	10.1	(0.40)	28	(1.10)	2.75
Heat-affected zone (center)		X	X	-	15.2	(0.60)	30.5	(1.20)	2
Heat-affected zone (boundary)		X	X	X	14	(0.55)	28	(1.10)	2.75

[a] X = test performed; SLC = static load cracking test.

Table 5. Fracture toughness of Ti-6Al-4V base metal specimens in the ML orientation. (Specimen thickness B = 20.3 at T = 76 K; B = 25.4 at T > 76 K)

Temperature K	Temperature (°F)	Specimen Number	Orientation	a/W	$2.5\,(K_Q/\sigma_y)^2$ mm	K_Q $MN/m^{3/2}$	K_{Ic} $MN/m^{3/2}$	K_{Ic} $ksi\cdot in^{1/2}$
295	(70)	2	ML	.500	30	91.4	$K_Q \neq K_{Ic}$	
		3	ML	.525		84.7	"	
		63	ML	.570		94.0	"	
		67	ML	.655		93.9	"	
195	(-109)	57	ML	.555	19	$K_Q \approx K_{Ic}$	91.4	83.1
		69	ML	.530		$K_Q = K_{Ic}$	87.5	79.6
176	(-143)	60	ML	.515	19	$K_Q = K_{Ic}$	95.6	87.0
130	(-226)	4	ML	.575	16	$K_Q \approx K_{Ic}$	86.4	78.6
		53	ML	.565		$K_Q \approx K_{Ic}$	95.6	87.0
		50	ML	.535		$K_Q = K_{Ic}$	95.6	87.0
108	(-266)	58	ML	.540	14	$K_Q = K_{Ic}$	85.6	77.9
76	(-323)	5	ML	.480	5	$K_Q = K_{Ic}$	65.0	59.1
		7	ML	.515		$K_Q = K_{Ic}$	60.8	55.3
		10	ML	.555		$K_Q \approx K_{Ic}$	65.6	59.7

Table 6. Fracture toughness of Ti-6Al-4V base metal specimens in the LR orientation. (Specimen thickness, B, = 20.3 mm)

Temperature K	Temperature (°F)	Specimen Number	Orientation	$\frac{a}{W}$	$2.5\ (K_Q/\sigma_y)^2$ mm	K_Q MN/m$^{3/2}$	K_{Ic} MN/m$^{3/2}$	K_{Ic} ksi·in$^{1/2}$
295	(70)	7	LR	0.580	28	77.5	$K_Q \neq K_{Ic}$	
		8	LR	0.580		83.2	"	
		9	LR	0.575		78.9	"	
		10	LR	0.585		82.3	"	
		15	LR	0.570		85.9	"	
		17	LR	0.575		88.5	"	
200	(-100)	20	LR	0.530	16.5	84.5[a]	$K_Q \neq K_{Ic}$	
125	(-235)	19	LR	0.480	17	$K_Q = K_{Ic}$	100	91.0
110	(-262)	18	LR	0.515	9.8	$K_Q = K_{Ic}$	78.0	71.0
76	(-323)	1	LR	0.515	5	$K_Q = K_{Ic}$	61.7	56.1
		2	LR	0.575		$K_Q \cong K_{Ic}$	61.0	55.5
		3	LR	0.645		$K_Q \cong K_{Ic}$	61.6	56.1
		4	LR	0.675		$K_Q \cong K_{Ic}$	59.9	54.5
4	(-453)	11	LR	0.570	3	$K_Q \cong K_{Ic}$	54.0	49.1
		12	LR	0.505		$K_Q = K_{Ic}$	53.7	48.9
		13	LR	0.455		$K_Q = K_{Ic}$	54.6	49.7

[a] invalid; P_{max}/P_Q exceeded 1.10.

Table 7. Fracture toughness of Ti-6Al-4V base metal at 76 K as a function of orientation. (Specimen thickness, B, = 20.3 to 25.4 mm)

Temperature K	Temperature (°F)	Specimen Number	Orientation	a/W	K_Q $MN/m^{3/2}$	K_{Ic} $MN/m^{3/2}$	K_{Ic} $ksi \cdot in^{1/2}$
76	(-323)	5	ML	.480	$K_Q = K_{Ic}$	65.0	59.1
		7	ML	.515	$K_Q = K_{Ic}$	60.8	55.3
		10	ML	.555	$K_Q \geq K_{Ic}$	65.6	59.7
		40	MR	.550	$K_Q = K_{Ic}$	65.3	59.4
		36	MR	.520	$K_Q = K_{Ic}$	61.7	56.1
		48	MR	.490	$K_Q = K_{Ic}$	59.1	53.8
		31	LR[a]	.515	$K_Q = K_{Ic}$	60.9	55.4
		35	LR	.500	$K_Q = K_{Ic}$	59.9	54.5
		41	LR	.520	$K_Q = K_{Ic}$	56.0	51.0
		32	LM	.530	$K_Q = K_{Ic}$	61.3	55.8
		34	LM	.540	$K_Q = K_{Ic}$	59.9	54.5
		42	RM	.525	$K_Q = K_{Ic}$	58.3	53.0
		39	RM	.515	$K_Q = K_{Ic}$	65.9	60.0
		38	RL	.625	$K_Q \geq K_{Ic}$	57.4	52.2
		37	RL	.525	$K_Q = K_{Ic}$	54.6	49.7

[a] also see Table 6.

Table 8. Effect of thermal-mechanical treatments on the fracture toughness of Ti-6Al-4V (ELI) base metal.

Treatment prior to test	Test Temperature K	Test Temperature (°F)	Specimen Number	Orientation	Thickness mm	K_{Ic} $MN/m^{3/2}$	K_{Ic} $ksi \cdot in^{1/2}$
SRA[a]: 533 K (500°F), 50 h	76	(-323)	11	MR	20.3	58.0	52.8
			12	MR	20.3	67.6	61.5
SRA: 811 K (1000°F), 50 h	76	(-323)	13	ML	25.4	60.9	55.4
			14	ML	25.4	65.4	59.5
Prestrained in biaxial tension	295	(70)	11	ML	15.7	52.0	47.3
			22	LM	15.7	55.1	50.1
	76	(-323)	33	ML	15.7	51.2	46.6
			44	LM	15.7	51.6	47.0

[a] Simulated stress-relief anneal, conducted in air.

Table 9. Fracture toughness of stress-relief annealed Ti-6Al-4V electron beam welds.

Location	Temperature K	Temperature (°F)	Specimen Number	Thickness mm	a/W	Orientation	$2.5(K_Q/\sigma_y)^2$ mm	K_Q MN/m$^{3/2}$	K_{Ic} MN/m$^{3/2}$	K_{Ic} ksi·in$^{1/2}$
Fusion Zone (FZ)	295	(70)	7	14	.520	MR	22	76.8	$K_Q \neq K_{Ic}$	
			8	14	.470	MR		78.5		
	76	(-323)	2	14	.475	MR	4	$K_Q = K_{Ic}$	59.1	57.8
			3	14	.505	MR		$K_Q = K_{Ic}$	64.9	59.1
			4	14	.515	MR		$K_Q = K_{Ic}$	55.0	50.0
			10	10.1	.475	ML	4	$K_Q = K_{Ic}$	55.3	50.3
			55	14	.470	ML		$K_Q = K_{Ic}$	61.4	55.9
			77	14	.475	ML		$K_Q = K_{Ic}$	55.1	50.1
			88	14	.560	ML		$K_Q \approx K_{Ic}$	56.3	51.2
Heat-Affected Zone (HAZ)	295	(70)	20	15.2	.500	MR	23	83.7	$K_Q \neq K_{Ic}$	
			22	15.2	.600	MR		81.8	$K_Q \neq K_{Ic}$	
			23	15.2	.465	MR		72.4	$K_Q \neq K_{Ic}$	
	76	(-323)	25	15.2	.535	MR	4	$K_Q = K_{Ic}$	58.2	53.0
			26	15.2	.420	MR		$K_Q = K_{Ic}$	57.6	52.4
			27	15.2	.490	MR		$K_Q = K_{Ic}$	55.7	50.7
HAZ/FZ Boundary (HAZB)	295	(70)	4	10.1	.595	MR	16	63.7	$K_Q \neq K_{Ic}$	
			1	10.1	.560	MR		70.3	$K_Q \neq K_{Ic}$	
	76	(-323)	7	10.1	.485	MR	3	$K_Q = K_{Ic}$	53.1	48.3
			9	10.1	.435	MR		$K_Q = K_{Ic}$	52.3	47.6
			12	10.1	.495	MR		$K_Q = K_{Ic}$	47.5	43.2

Table 10. Static load cracking tests of electron beam welded Ti-6Al-4V specimens.

Specimen and crack location		Temperature K	Temperature (°F)	Stress Intensity Factor, K $MN/m^{3/2}$	Stress Intensity Factor, K $(ksi \cdot in^{1/2})$	Hold Time, Δt sec.	Hold Time, Δt (h)	Result
Fusion zone	11	76	(-323)	56.9	(51.8)	18,000	(5)	No measurable crack growth
	13	76		55.1	(50.2)	36,000	(10)	
	12	295	(70)	73.9	(67.3)	36,000	(10)	Δa = 1.10 mm (crack arrest)
	17	295		73.4	(66.8)	1,560	(0.43)	Δa = 1.29 mm (crack arrest)
	10	295		68.1	(62.0)	3.42×10^5	(95)	Δa = .51 mm (crack arrest)
	15	295		61.5	(56.0)	3.42×10^5	(95)	No measurable crack growth
	14	295		56.1	(51.1)	3.42×10^5	(95)	No measurable crack growth
	16	295		51.0	(46.4)	4.18×10^5	(116)	No measurable crack growth
HAZ/FZ boundary	7	76	(-323)	50.1	(45.6)	58,000	(16)	No measurable crack growth
	12	76		49.4	(45.0)	18,000	(5)	
	6	295	(70)	71.0	(64.6)	60	(0.17)	Δa = 0.30 mm
	1	295		69.9	(63.6)	20	(5.5×10^{-3})	Fracture
	2	295		69.0	(62.8)	1020	(2.83×10^{-1})	Fracture
	5	295		68.1	(62.0)	3.6×10^5	(100)	No measurable crack growth
	3	295		64.0	(58.3)	60	(1.7×10^{-2})	Δa = 0.32 mm
	4	295		60.4	(55.0)	50	(1.4×10^{-2})	Fracture

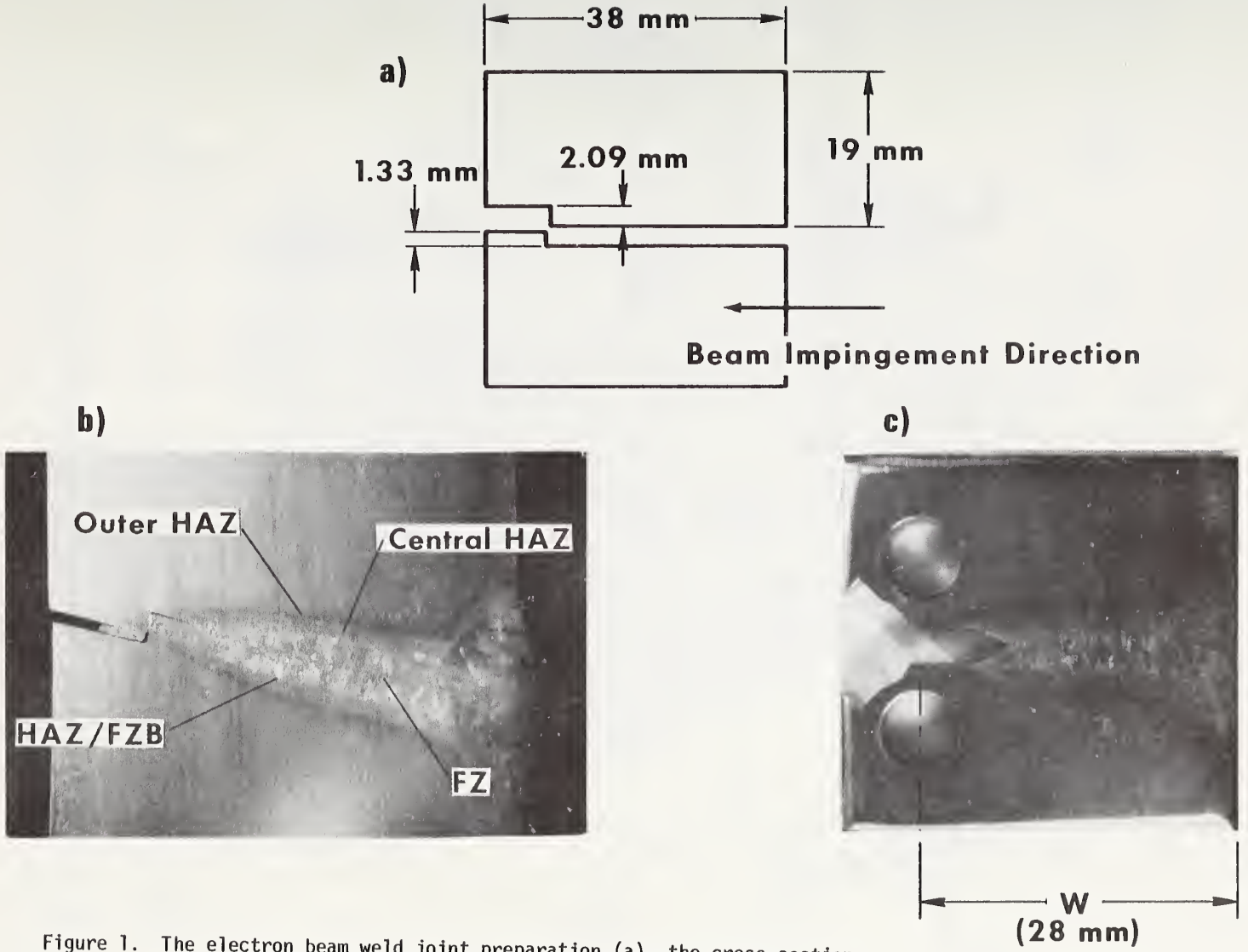

Figure 1. The electron beam weld joint preparation (a), the cross-section of a completed weld (b), and a compact specimen of the ML orientation (c).

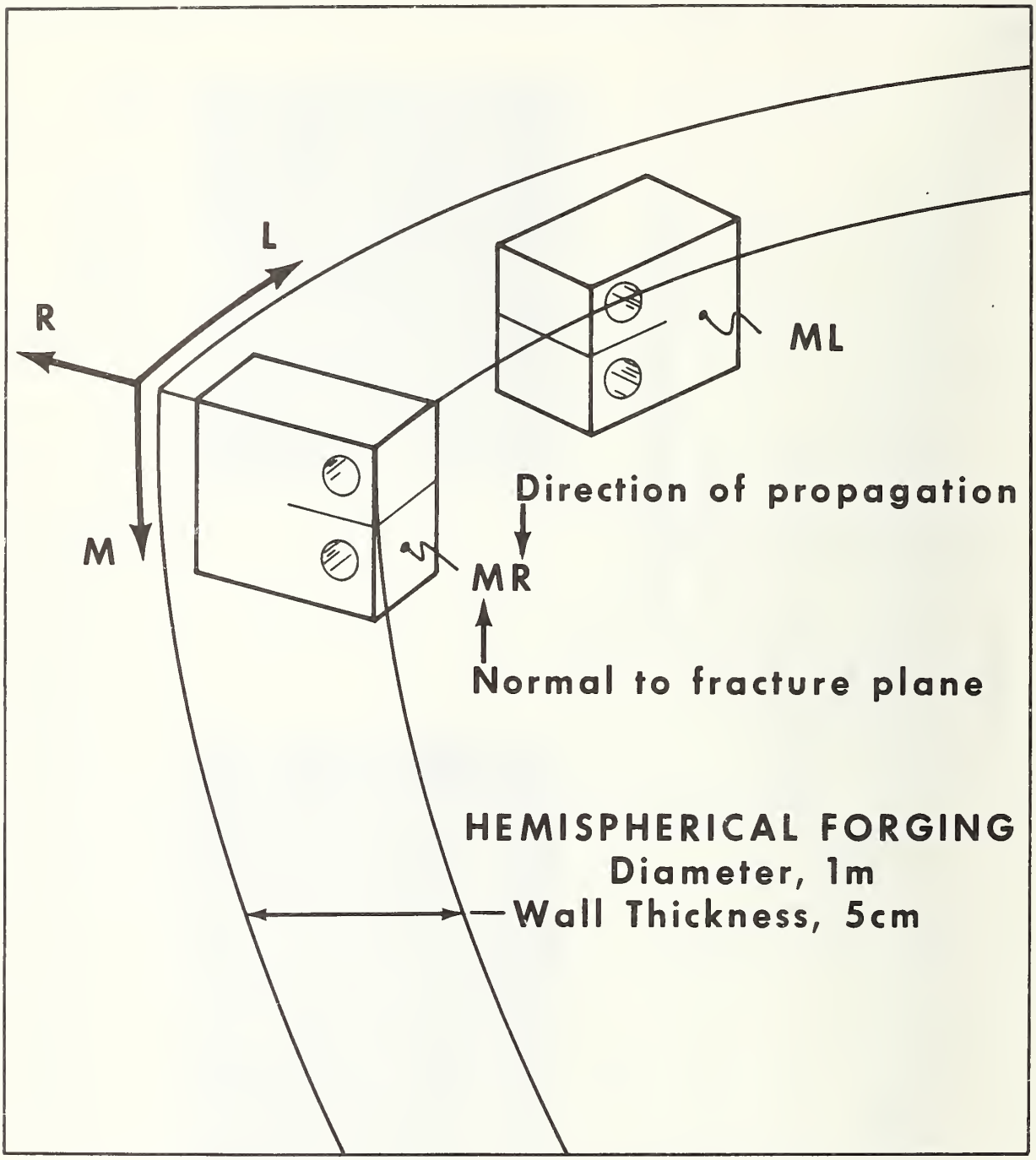

Figure 2. Notation for reference axes and specimen orientations.

Figure 3. The recrystallization annealed base metal microstructure, 340X.

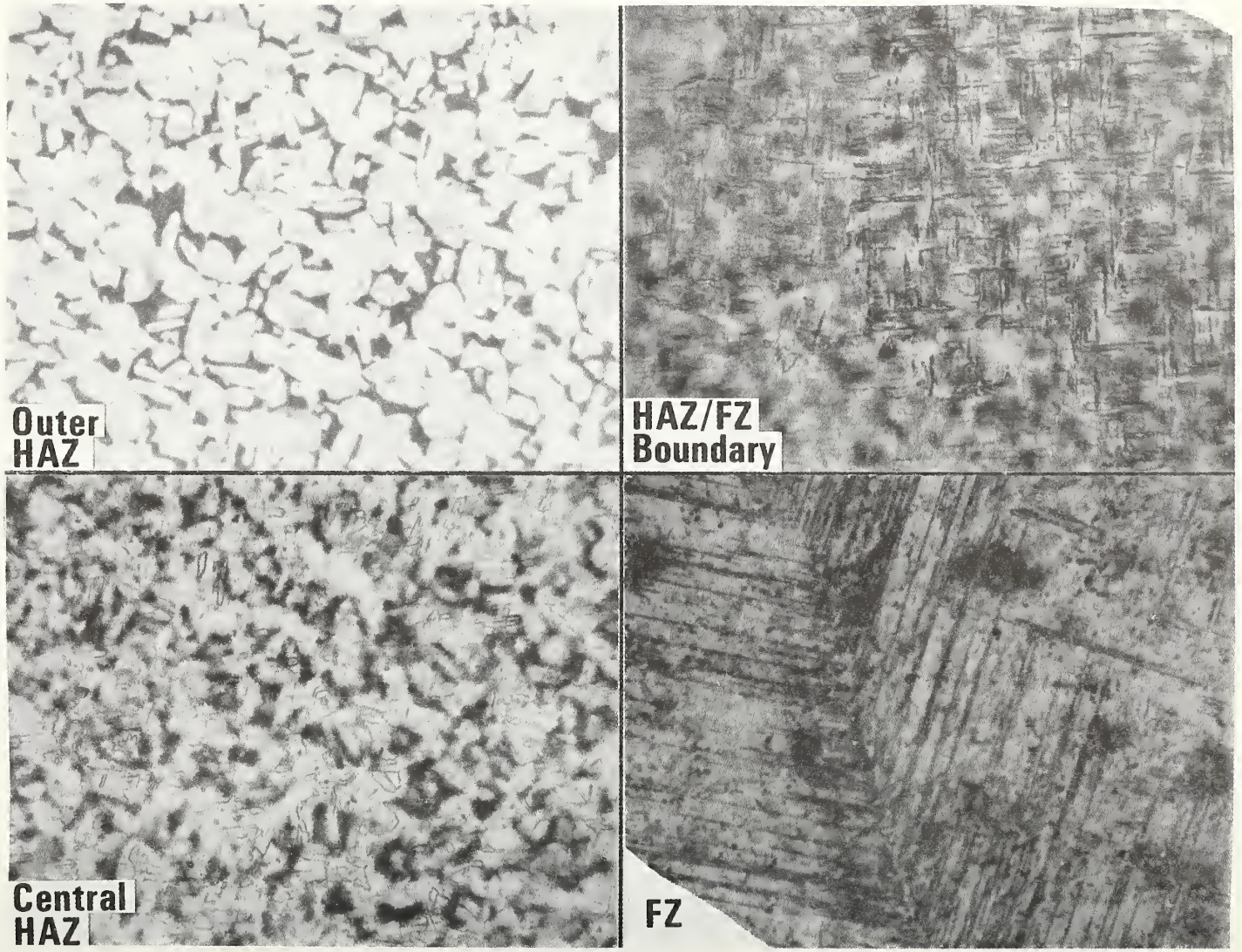

Figure 4. Electron beam weld microstructures, 340X.

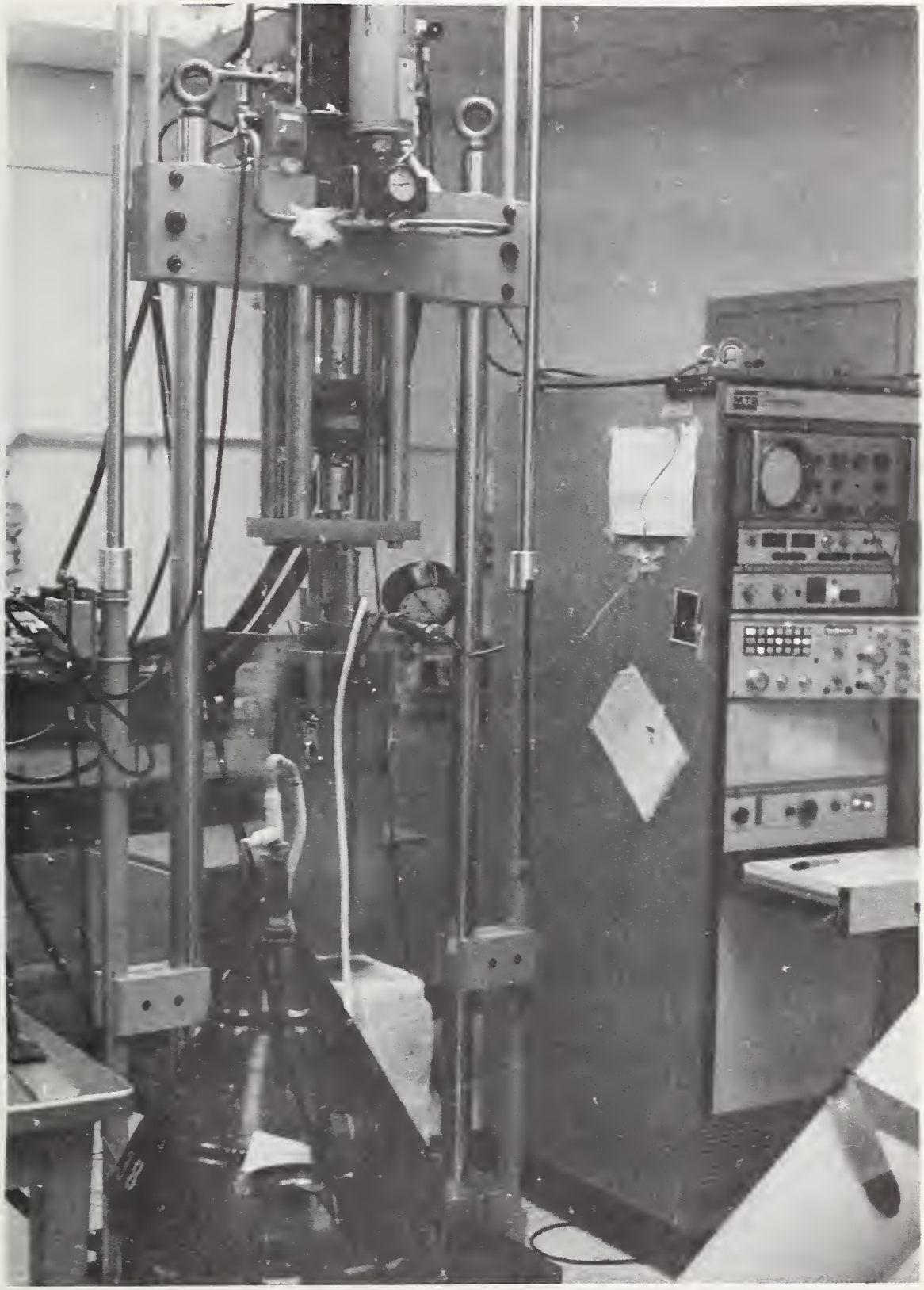

Figure 5. Low temperature fatigue and fracture testing apparatus.

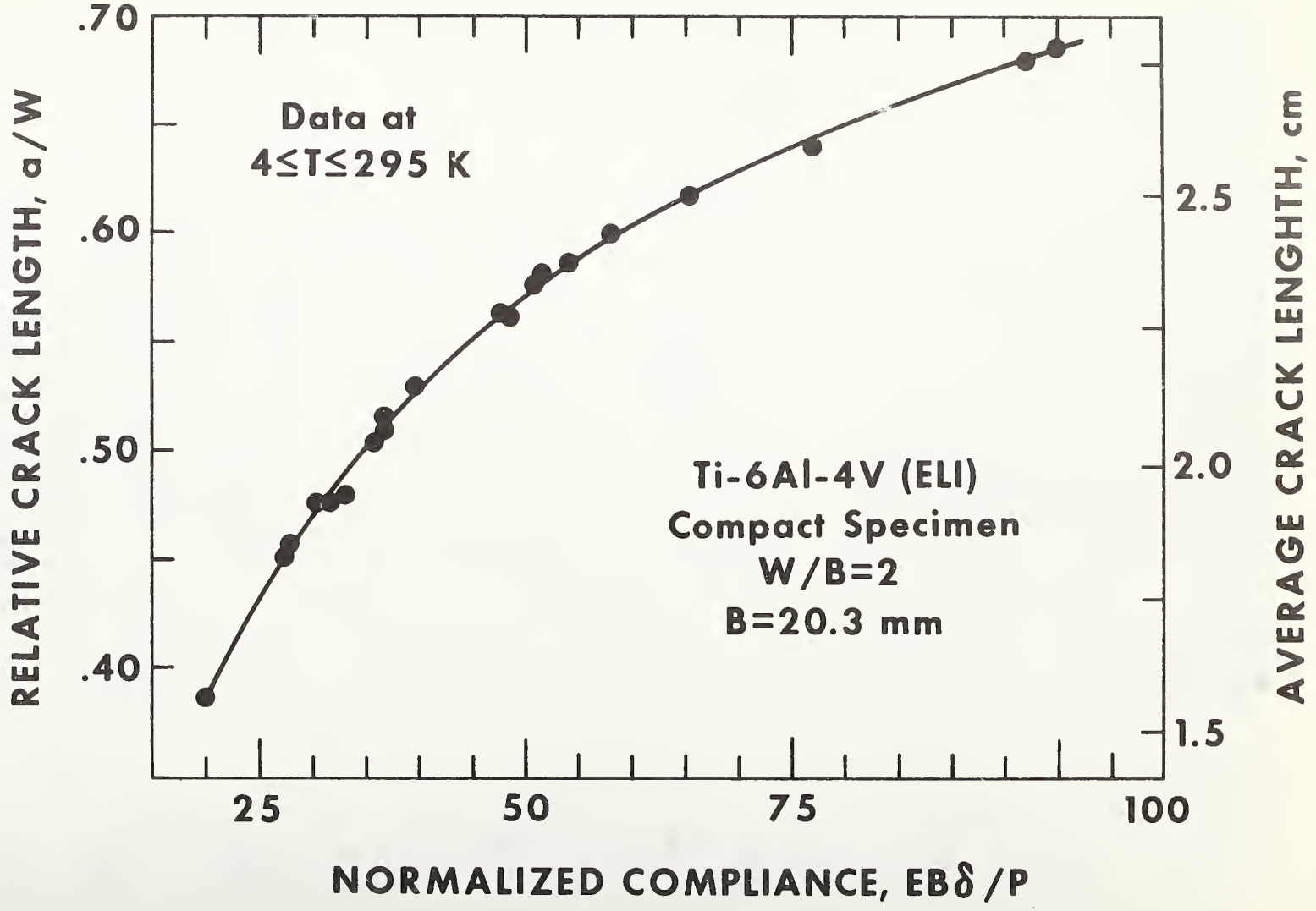

Figure 6. A typical crack-length/compliance correlation, used in crack growth measurements.

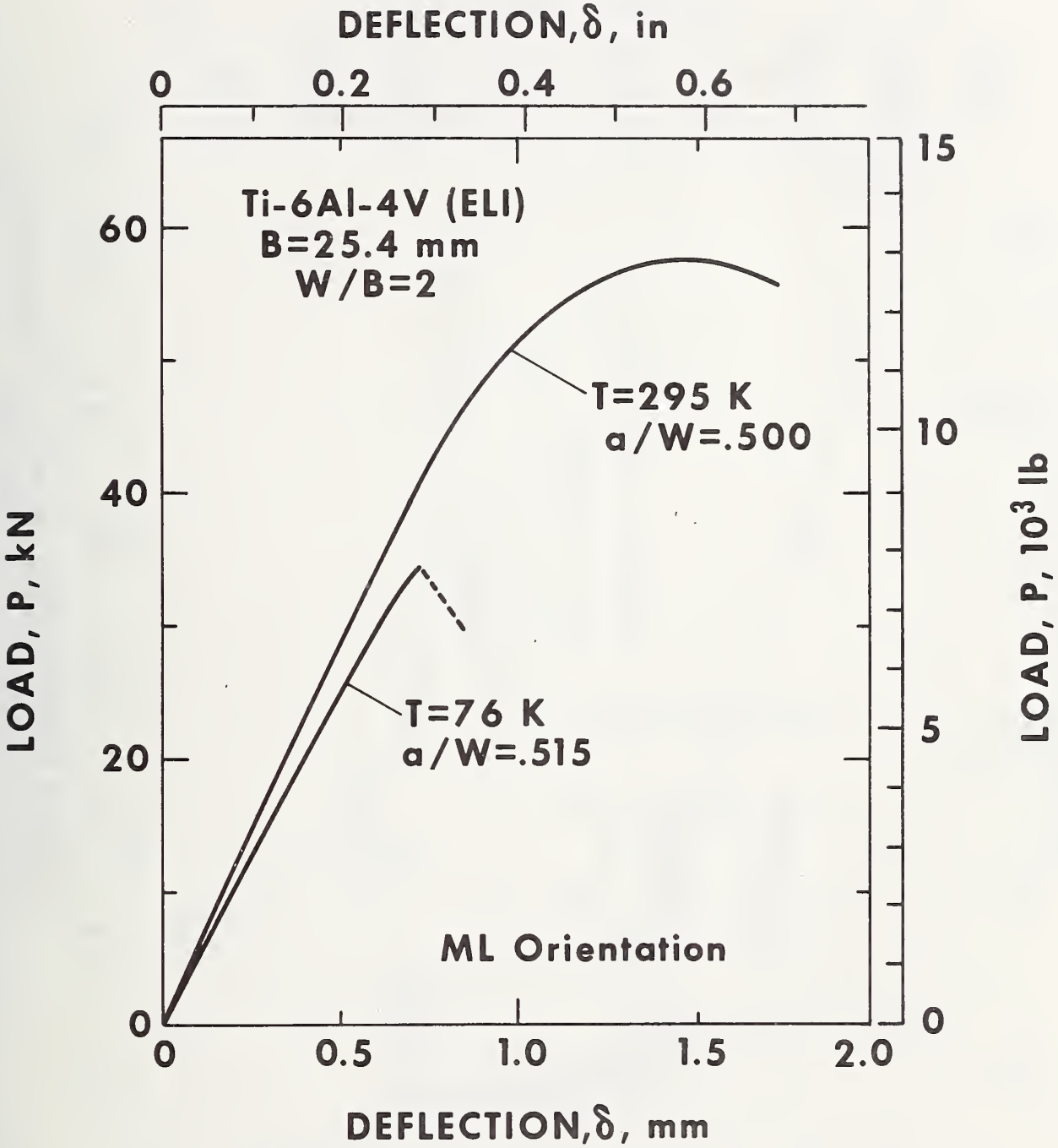

Figure 7. ASTM E 399-74 fracture test records for the base metal at 295 and 76 K.

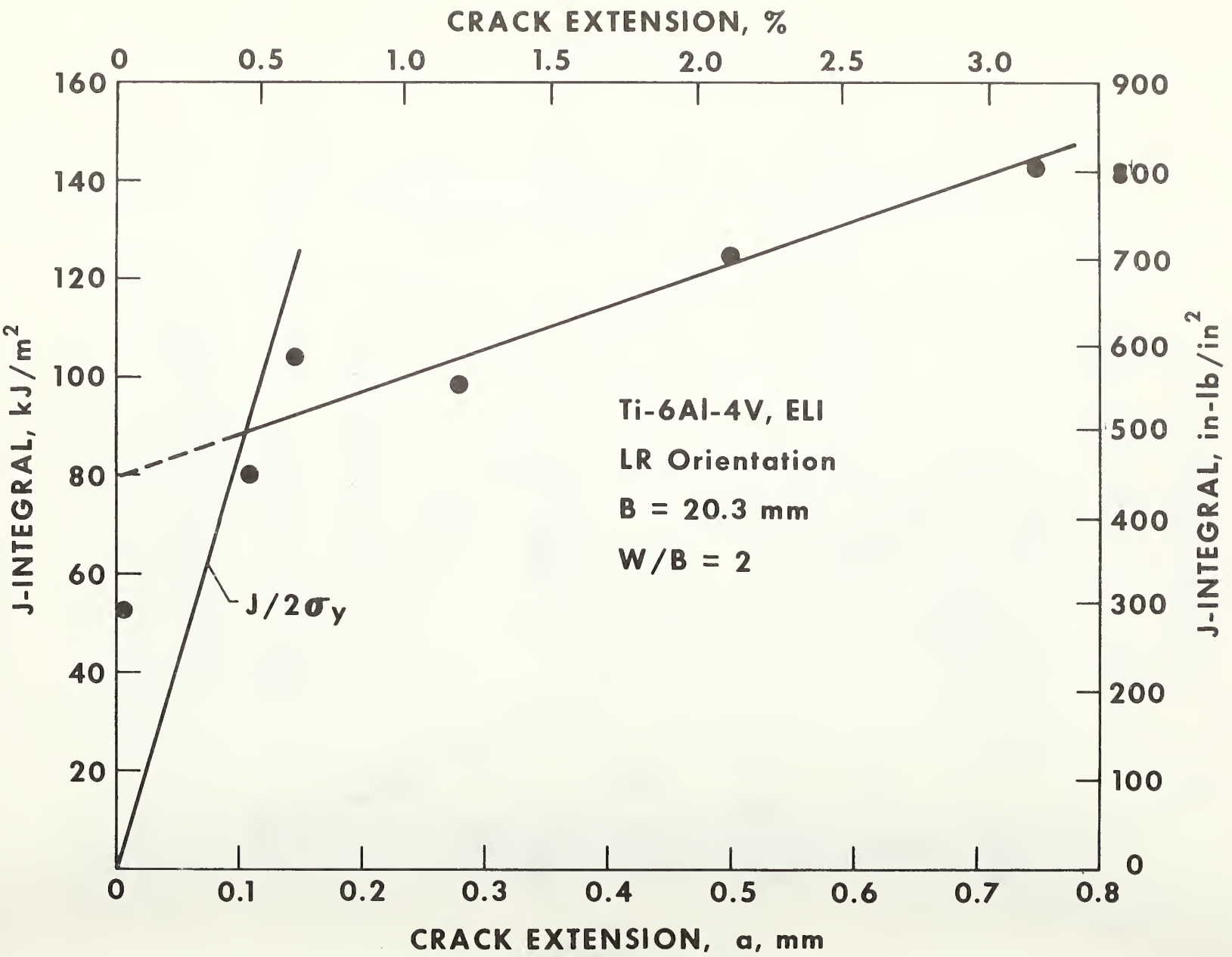

Figure 8. J-versus-Δa curve for the base metal at room temperature.

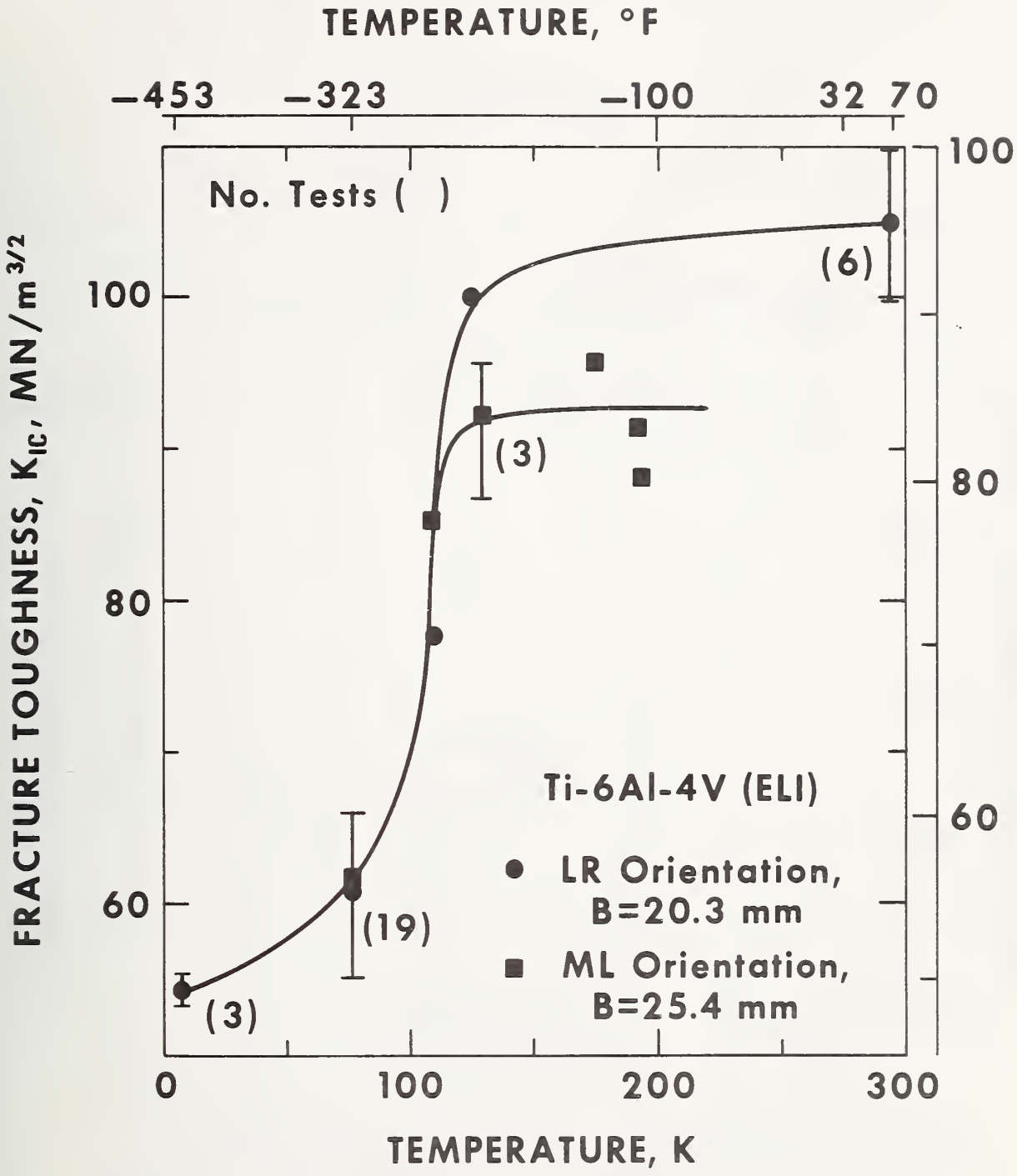

Figure 9. The temperature dependence of K_{IC} for the base metal, indicating transitional behavior at 76 K $\leq$ T $\leq$ 125 K.

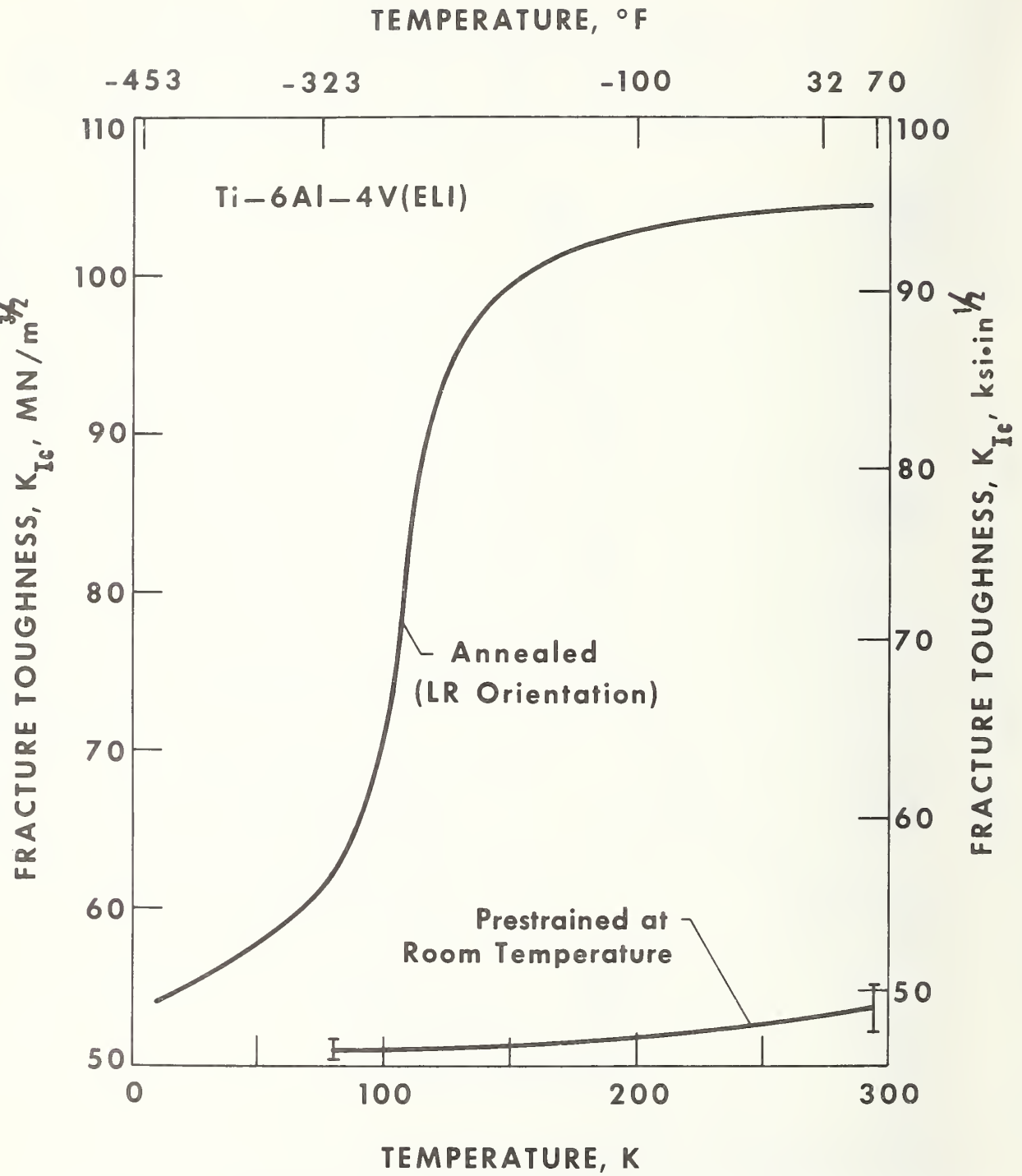

Figure 10. The effect of a room temperature prestrain in biaxial tension on the fracture toughness of the base metal.

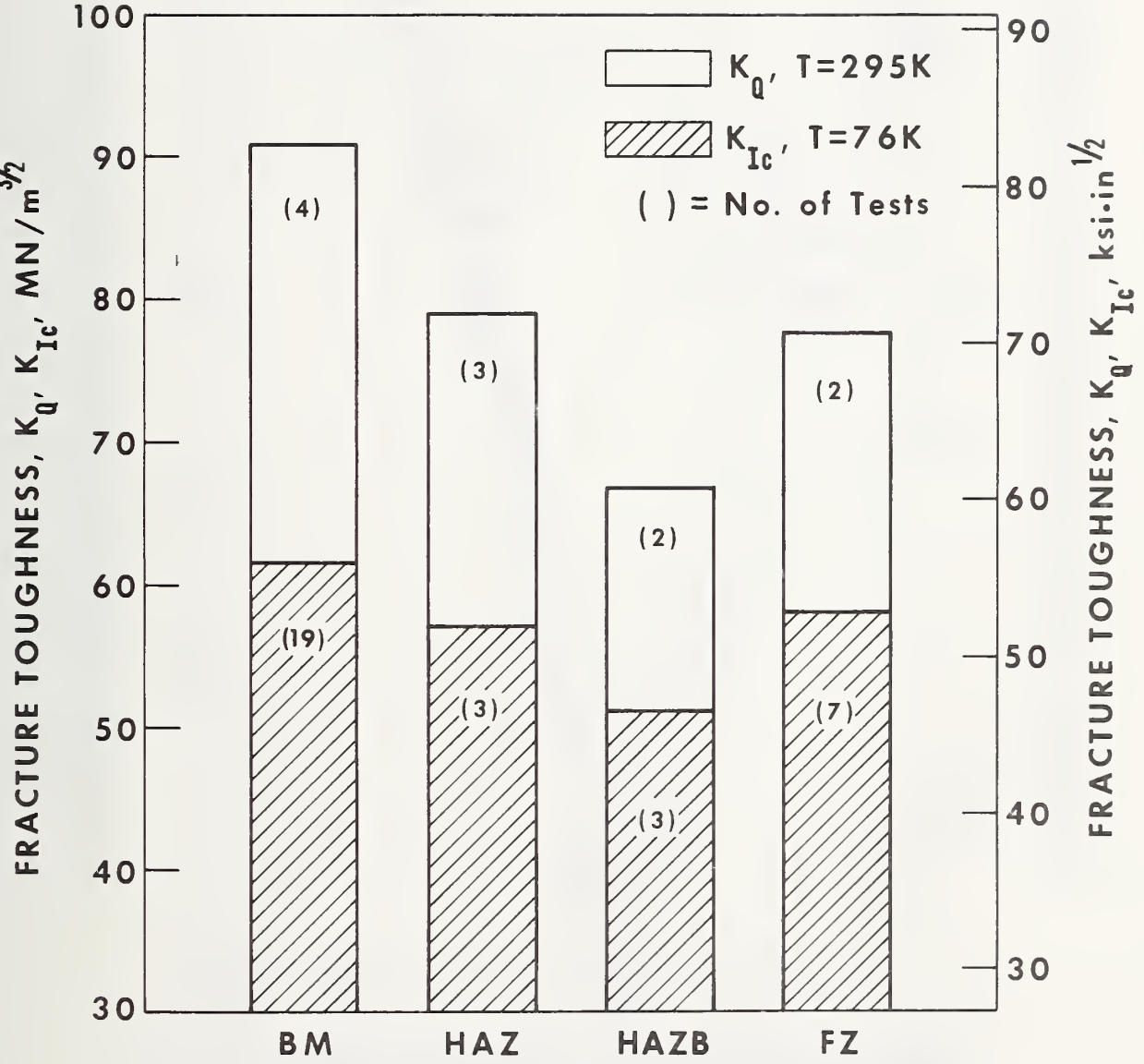

Figure 11. The average fracture toughness as a function of crack location in the Ti-6Al-4V base metal and its electron beam welds.

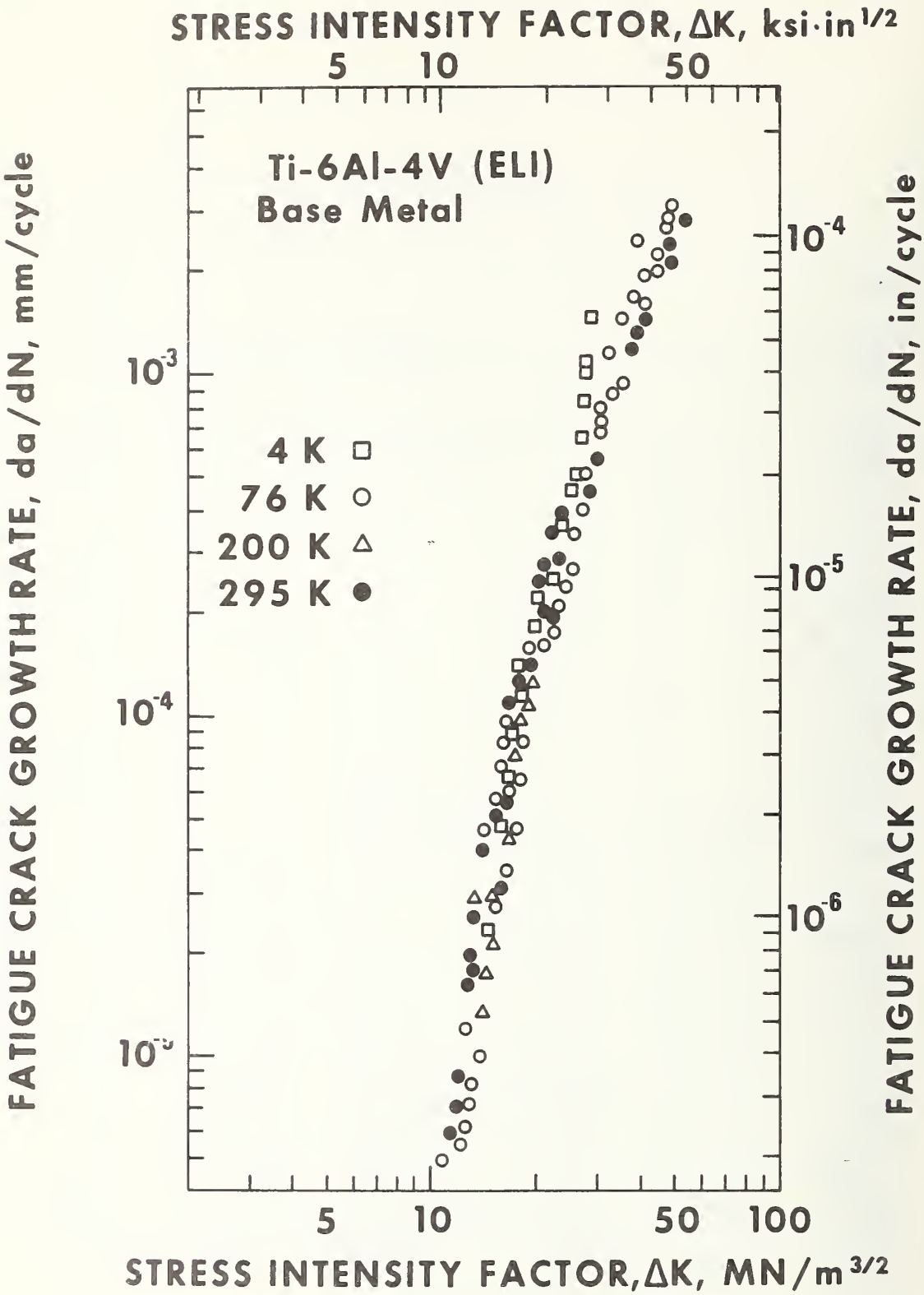

Figure 12. Fatigue crack growth rates for base metal specimens of the LR orientation [11].

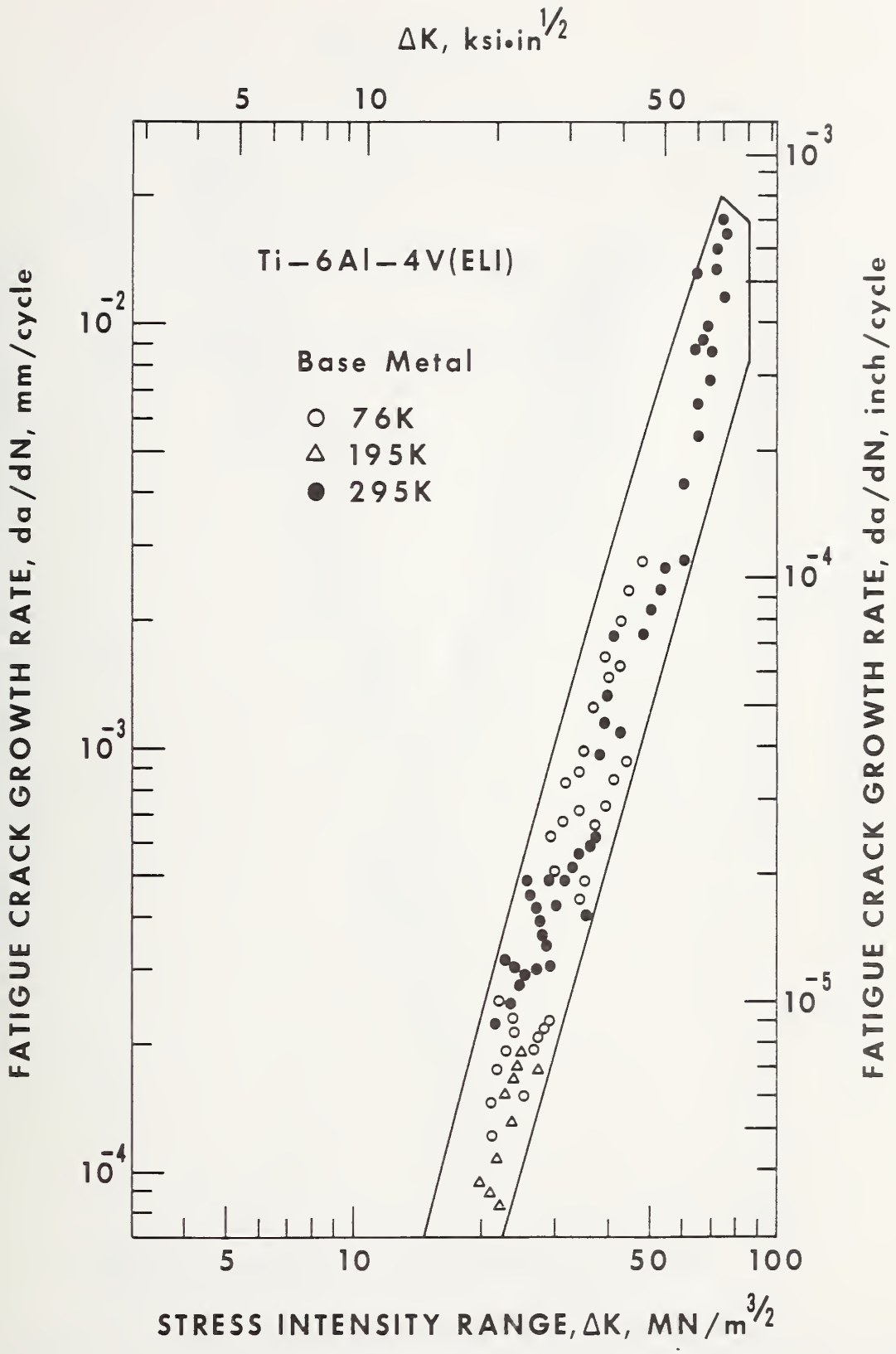

Figure 13. Fatigue crack growth rates for base metal specimens, primarily of the ML orientation.

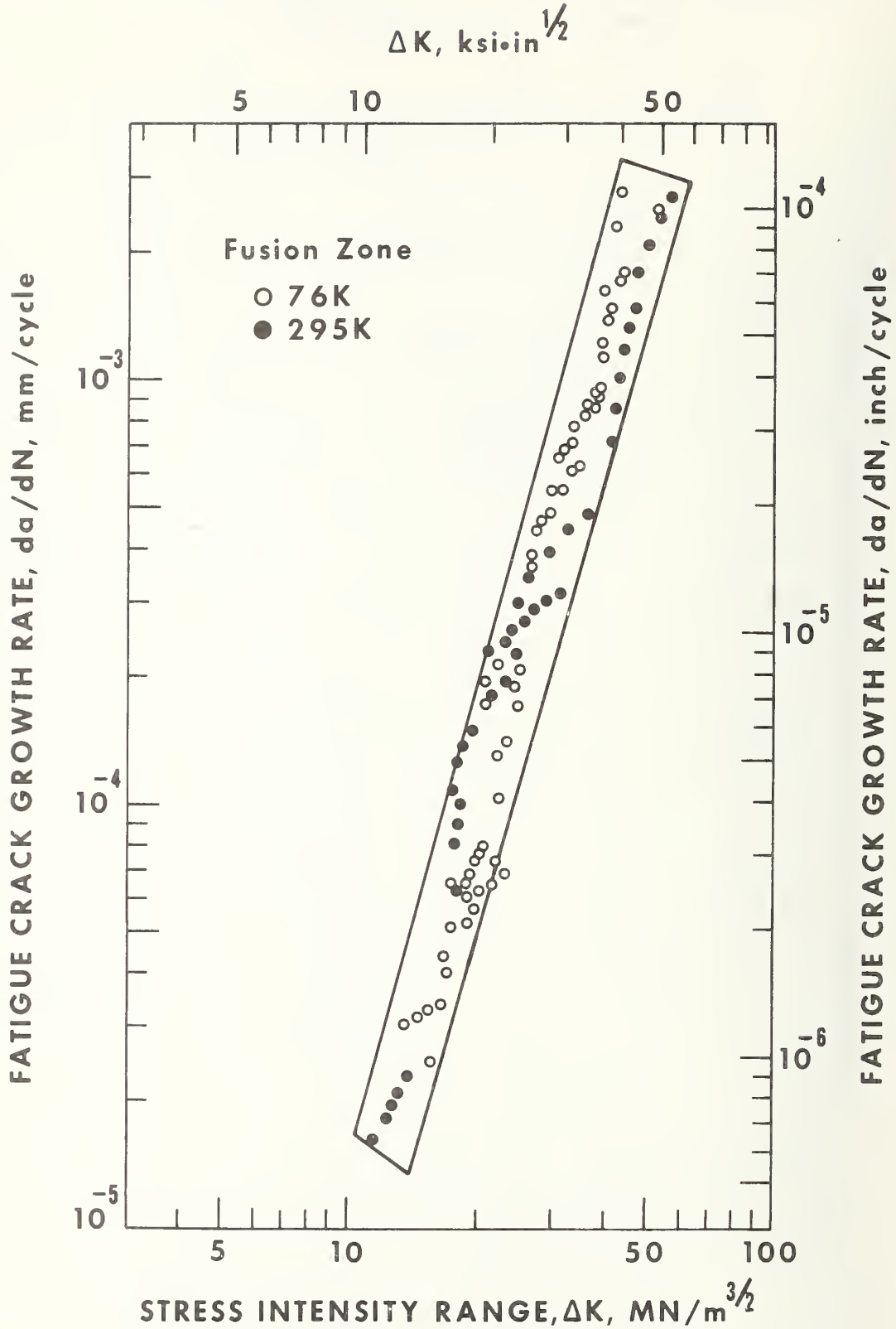

Figure 14. Fatigue crack growth rates for electron beam weld fusion zone specimens of the MR orientation.

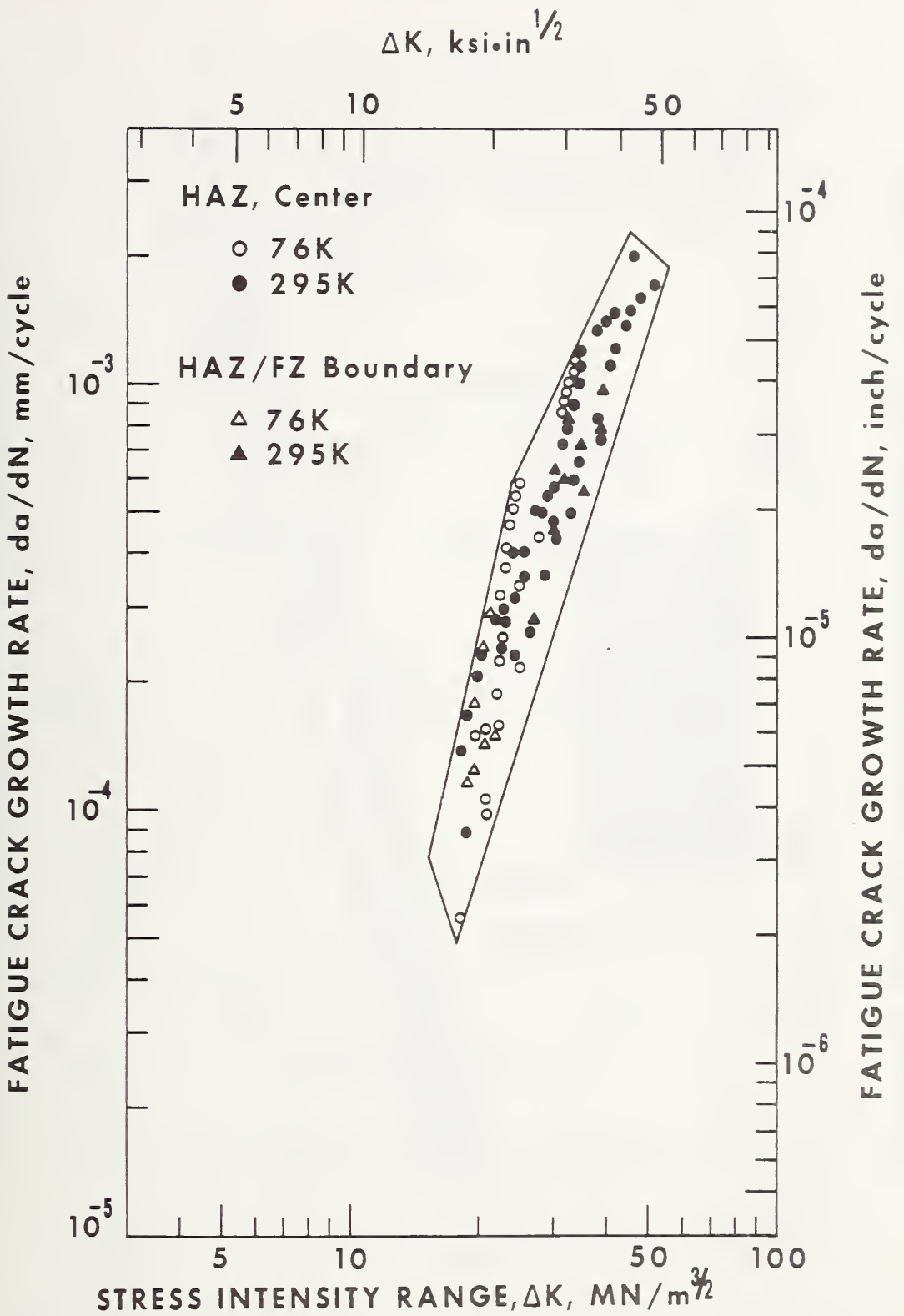

Figure 15. Fatigue crack growth rates for heat-affected zone specimens of the MR orientation with cracks sited near the center (HAZ) and boundary (HAZB).

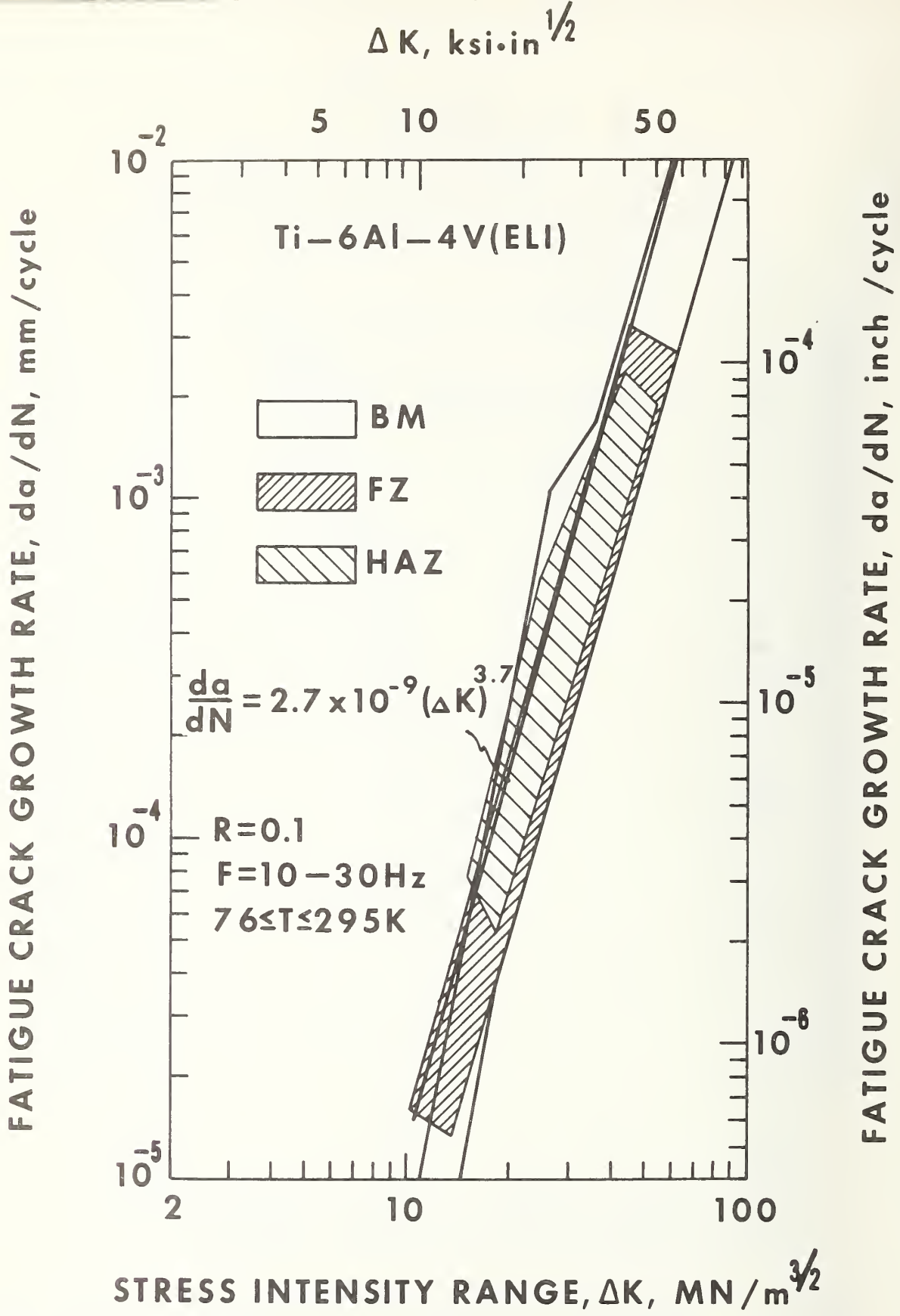

Figure 16. A comparison of fatigue crack growth rate scatterbands for base metal and weld zones.

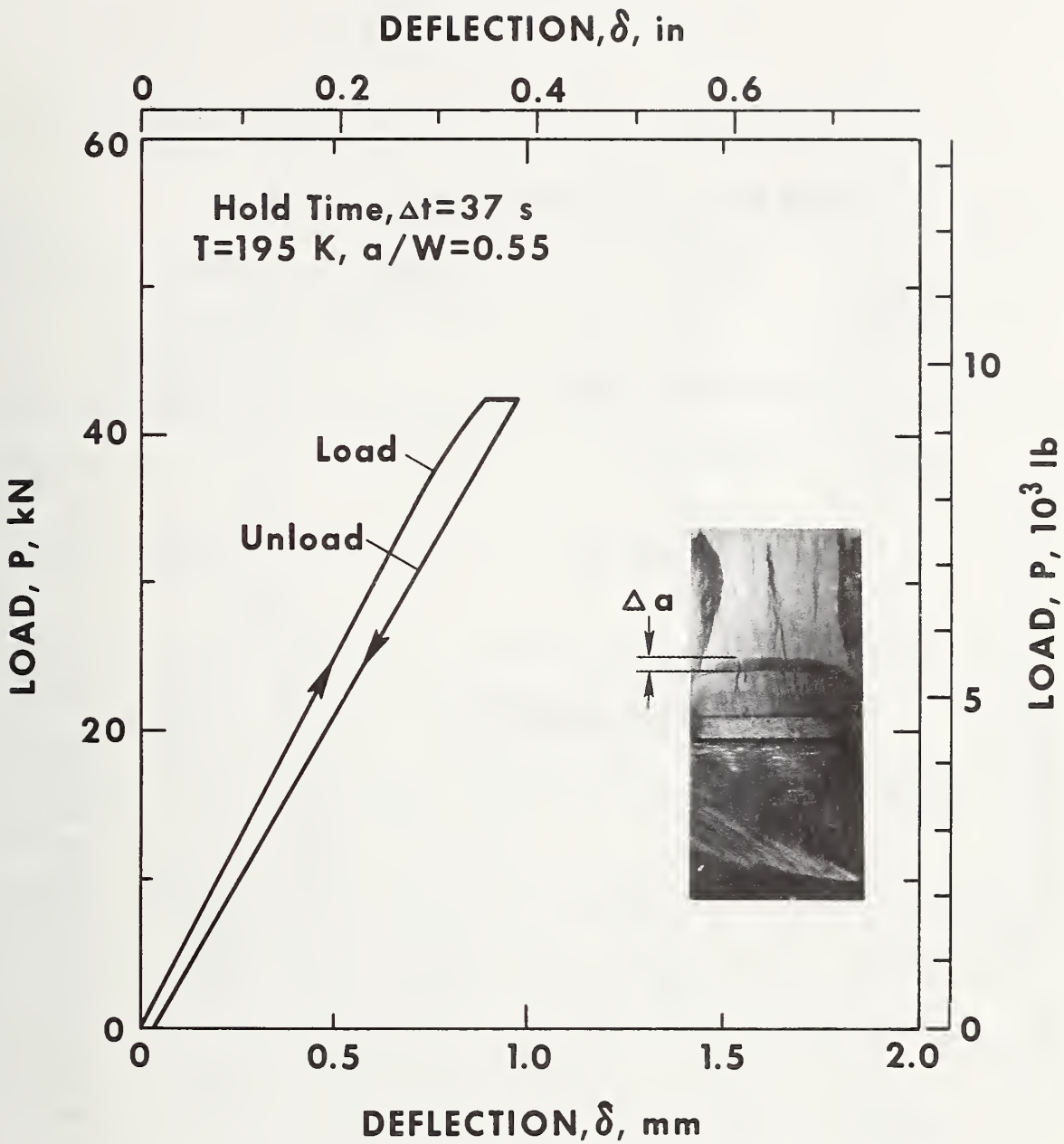

Figure 17. Static load fracture behavior of the base metal, showing the compact specimen fracture surface.

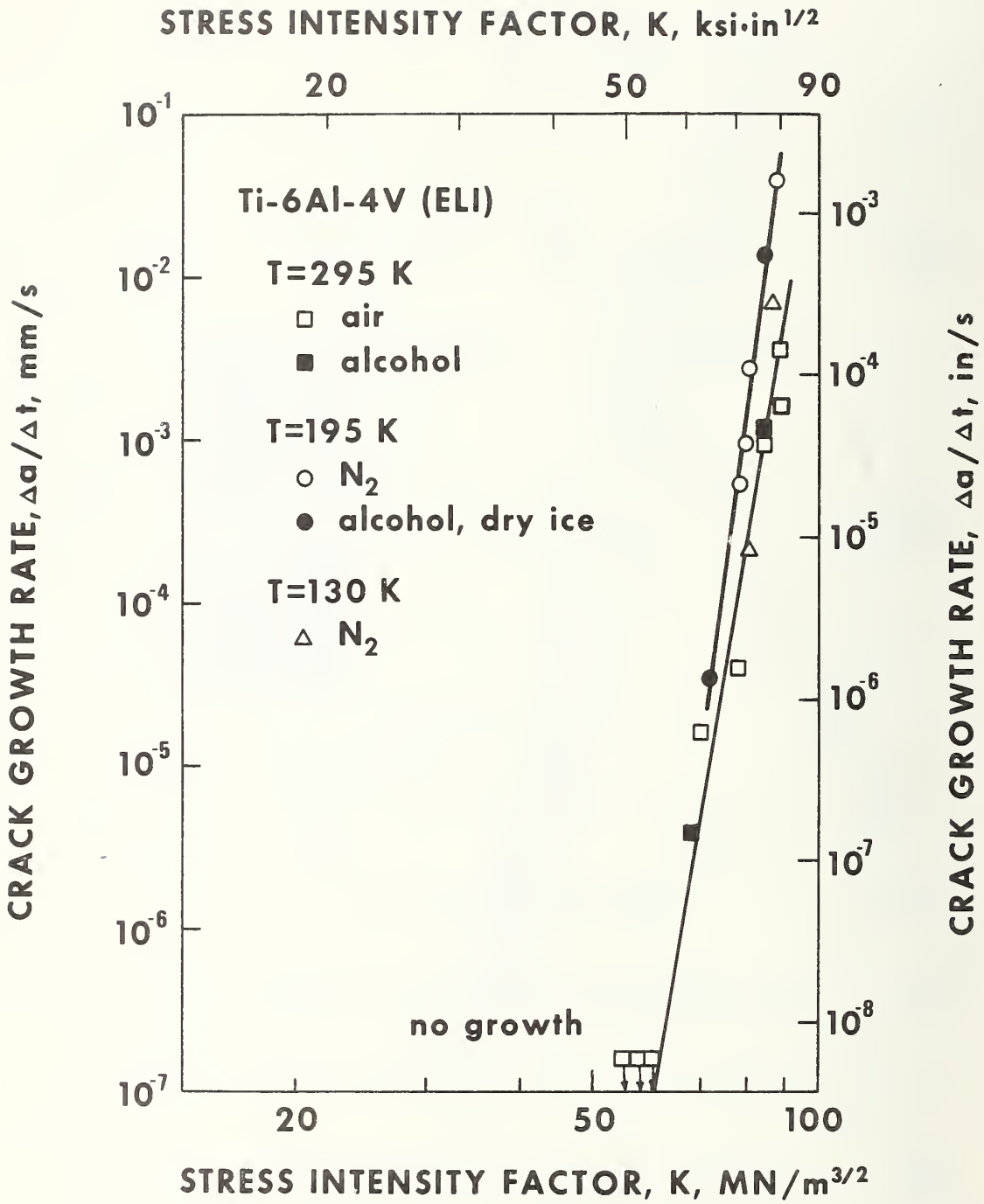

Figure 18. Static load cracking rates for the base metal at room and cryogenic temperatures.

NBS-114A (REV. 7-73)

U.S. DEPT. OF COMM. BIBLIOGRAPHIC DATA SHEET	1. PUBLICATION OR REPORT NO. NBSIR 76-836	2. Gov't Accession No.	3. Recipient's Accession No.

4. TITLE AND SUBTITLE

Low Temperature Fracture Behavior of a Ti-6Al-4V Alloy and its Electron Beam Welds

5. Publication Date: April 1976

6. Performing Organization Code: 275.03

7. AUTHOR(S)

R. L. Tobler

8. Performing Organ. Report No.

9. PERFORMING ORGANIZATION NAME AND ADDRESS

NATIONAL BUREAU OF STANDARDS
DEPARTMENT OF COMMERCE
WASHINGTON, D.C. 20234

10. Project/Task/Work Unit No.: 2750431

11. Contract/Grant No.: AFWL/75-PO-177

12. Sponsoring Organization Name and Complete Address (*Street, City, State, ZIP*)

Kirtland AFB
Albuquerque, NM 87117

13. Type of Report & Period Covered: FY 1975

14. Sponsoring Agency Code

15. SUPPLEMENTARY NOTES

16. ABSTRACT (*A 200-word or less factual summary of most significant information. If document includes a significant bibliography or literature survey, mention it here.*)

The effects of electron beam (EB) welding on the fracture behavior of a recrystallization annealed, extra-low-interstitial Ti-6Al-4V alloy have been investigated at temperatures in the ambient-to-cryogenic range. Plane strain fracture toughness (K_{Ic}) and subcritical crack growth parameters were measured using compact specimens 10 to 25.4 mm-thick. These parameters can be used to predict the safe operating lifetimes of cryogenic pressure vessels and other welded Ti-6Al-4V structures.

Although EB welding transforms the base metal microstructure extensively, its effects on the material's fatigue crack propagation resistance at intermediate stress intensity factors are negligible. The growth rates, da/dN, of fatigue cracks sited in the fusion and heat-affected zones of weldments were temperature insensitive and nearly equivalent to rates for the base metal. However, welding introduces a zone of low fracture toughness at the heat-affected-zone/fusion-zone boundary. The K_{Ic} value for this boundary zone at liquid nitrogen temperature (76 K) was 45 $MN/m^{3/2}$, 16% lower than the base metal. The base metal fracture toughness increases between 4 and 295 K, with an abrupt transition to higher K_{Ic} values occurring at temperatures between 76 and 125 K. Static load cracking, temperature effects, and specimen orientation effects on the fracture behavior of this titanium alloy are central topics of discussion.

17. KEY WORDS (*six to twelve entries; alphabetical order; capitalize only the first letter of the first key word unless a proper name; separated by semicolons*)

Electron beam welding; fatigue; fracture toughness; low temperature tests; mechanical properties; titanium alloy.

18. AVAILABILITY

[X] Unlimited

[ ] For Official Distribution. Do Not Release to NTIS

[ ] Order From Sup. of Doc., U.S. Government Printing Office Washington, D.C. 20402, SD Cat. No. C13

[X] Order From National Technical Information Service (NTIS) Springfield, Virginia 22151

19. SECURITY CLASS (THIS REPORT): UNCLASSIFIED

21. NO. OF PAGES: 45

20. SECURITY CLASS (THIS PAGE): UNCLASSIFIED

22. Price: $3.75